Genetic polymorphisms in *COMT* and *BDNF* influence synchronization dynamics of human neuronal oscillations

Jaana Simola [*1,2,3¶], Felix Siebenhühner [1¶], Vladislav Myrov [1,4], Katri Kantojärvi [5,6], Tiina Paunio [5,6], J. Matias Palva [1,4,7], Elvira Brattico [8, 9&] & Satu Palva [*1,7&]

[1] Neuroscience Center, Helsinki Institute of Life Science, University of Helsinki, P.O. Box 21, (Haartmaninkatu 3), FI-00014 Helsinki, Finland

[2] Helsinki Collegium for Advanced Studies (HCAS), University of Helsinki, Finland

[3] BioMag Laboratory, HUS Medical Imaging Centre, FI-00029 HUS, Finland.

[4] Department of Neuroscience and Bioengineering (NBE), Aalto University, 02150 Espoo, Finland

[5] Genomics and Biomarkers Unit, Finnish Institute for Health and Welfare, Helsinki, FI-00271 Helsinki, Finland

[6] Department of Psychiatry and SleepWell Research Program, Faculty of Medicine, University of Helsinki and Helsinki University Central Hospital, Helsinki, FI-00014 Helsinki, Finland

[7] Centre for Cognitive Neuroimaging (CCNi), Institute of Neuroscience and Psychology, University of Glasgow, Glasgow G12 8QB, UK.

[8] Center for Music in the Brain (MIB), Department of Clinical Medicine, Aarhus University & The Royal Academy of Music Aarhus/Aalborg, 8000 Aarhus C, Denmark

[9] Department of Education, Psychology, Communication, University of Bari Aldo Moro, 70121 Bari, Italy

* Corresponding authors:

E-mail: jaana.simola@helsinki.fi (JS); satu.palva@helsinki.fi (SP)

¶These authors contributed equally to this work.

&These authors also contributed equally to this work.

Abbreviations

5-HT = 5-hydroxytryptamine

DA = dopamine

DAN = Dorsal attention network

DMN = Default Mode network

FPN = Frontoparietal network

Lim = Limbic system

NE = noradrenaline

SM= Somatomotor network

VAN = Ventral attention network

Vis = Visual network

Abstract

Neuronal oscillations, their inter-areal synchronization and scale-free dynamics constitute fundamental mechanisms for cognition by regulating communication in neuronal networks. These oscillatory dynamics have large inter-individual variability that is partly heritable. However, the genetic underpinnings of oscillatory dynamics have remained poorly understood. We recorded resting-state magnetoencephalography (MEG) from 82 participants and investigated whether oscillation dynamics were influenced by genetic polymorphisms in Catechol-O-methyltransferase (*COMT*) Val^{158}Met and brain-derived neurotrophic factor (*BDNF*) Val^{66}Met. Both *COMT* and *BDNF* polymorphisms influenced local oscillation amplitudes and their long-range temporal correlations (LRTCs), while only *BDNF* polymorphism affected the strength of large-scale synchronization. Brain criticality framework and computational modelling of near-critical synchronization dynamics suggested that *COMT* and *BDNF* polymorphisms influenced local oscillations via differences in net excitation-inhibition balance. Our findings demonstrate that *COMT* and *BDNF* genetic polymorphisms contribute to inter-individual variability in local and large-scale synchronization dynamics of neuronal oscillations.

Introduction

Spontaneous brain activity is characterized by neuronal oscillations from infra-slow (0.01–1 Hz) to high (200–600 Hz) frequency bands throughout the neuroanatomical scales from microcircuits to whole-brain networks. Sub-second time-scale oscillations (> 1 Hz) and their inter-areal synchronization play fundamental mechanistic roles in cognitive functions by regulating neuronal processing and communication across distributed brain areas [1-3]. In humans, dynamics of neuronal oscillations and their long-range phase synchronization, *i.e.*, electrophysiological functional connectivity (FC), that can be observed non-invasively in magneto- (MEG) and electroencephalography (EEG) recordings, serve fundamental roles in a variety of sensory, motor, and cognitive functions [4-8]. During rest, brain activity in sub-second time-scales is dominated by alpha oscillations [6], but involves frequency-specific inter-areal correlation structures throughout the 1–100 Hz range [9-14]. Importantly, the intrinsic spatial organization of spontaneous resting-state FCs observed both with MEG and functional magnetic resonance imaging (fMRI) is predictive of individual variability in task performance [12, 14-16], suggesting that such resting-state FC networks reflect underlying individual brain structural organization [17, 18].

Whole-brain modeling of multimodal neuroimaging data shows that neuromodulatory systems dynamically modulate the structural connectome over time, allowing flexible and complex computations [19]. Neuromodulation is involved in, *e.g.,* sustained attention, arousal, and vigilance, where it is associated with fluctuations in neuronal excitability [20, 21] in the time-scale of seconds to minutes. Catecholaminergic, dopamine (DA) and noradrenaline (NE) [22, 23], as well as the serotonergic (5-hydroxytryptamine; 5-HT) [20, 24, 25] neuromodulatory drive could constitute an important source for variability in neuronal dynamics by modulating oscillations either via changes of instantaneous activity state through common excitatory drive / gain or via dynamic state changes on slower timescales [20, 26-28].

In human MEG/EEG and intracranial electrophysiology, slow (0.1–1 Hz) and infra-slow (0.01–0.1 Hz) fluctuations are visible in scalp potentials and amplitude envelopes of fast > 1 Hz oscillations [9, 29, 30]. These fluctuations impact behavioral performance in sustained tasks [29]. Further, these fluctuations are scale-free*, i.e.* without a characteristic time-scale and exhibit power-law autocorrelations in their strength known as long-range-temporal correlations (LRTCs) [29, 31-35]. Similarly to instantaneous oscillations dynamics, inter-individual variability in neuronal LRTCs predicts variability in task-related behavioral LRCTs [35, 36].

A large fraction of variability in these neuronal dynamics could be heritable and explained by differences in genetic background. MEG spectral power shows similarities between siblings [37, 38]. Twin studies indicate that peak frequencies [39] as well as LRTCs of local cortical oscillations [40] have a genetic basis, so that up to 60% of the variance in neuronal LRTCs [40] and up to 85% of the variance in cognitive ability [41] can be attributed to genetic factors. However, what these genetic factors are and how they contribute to the inter-individual variability of synchronization dynamics, including oscillation amplitudes, large-scale synchronization, and LRTCs, have remained central unresolved questions.

Genetic polymorphism in the genes regulating the catabolism and re-uptake of the neurotransmitters could constitute an important source for this variability by modulating fluctuations of oscillations via their influence in the neuromodulator levels. Brain DA and NE levels are regulated by their catabolism via COMT enzyme [42, 43] of which activity is influenced by a common single-nucleotide polymorphism (SNP) in the *COMT* gene substituting methionine (Met) for valine (Val) at codon 158 at sequence 4680 ($Val^{158}Met$ (rs4680)). *COMT* Val^{158} homozygotes have higher COMT activity and therefore lower brain DA and NE levels than Met^{158} homozygotes, with activity for heterozygotes falling in the middle [44]. A considerable fraction of the variance in serotonin levels, on the other hand, is explained by $Val^{66}Met$ (rs6265) polymorphism of the gene

coding for BDNF, which influences 5-HT receptor binding [45] and the activity-dependent secretion of BDNF [46]. Compelling evidence indicates that *COMT* Val^{158}Met (rs4680) polymorphism is associated with modulation of neuronal activity in fMRI, especially in the prefrontal cortex (PFC) and with cognitive functions dependent on PFC [23, 47-49] while *BDNF* Val^{66}Met polymorphism is implicated in in many aspects of behavior and cognition [24, 25]. In addition to modulation 5-HT levels, activity-dependent release of BDNF also influences the maintenance and formation of neuronal networks [50, 51], thereby influencing cognition and behavior over lifetime.

We hypothesized here that *COMT* Val^{158}Met and *BDNF* Val^{66}Met polymorphisms could influence oscillation amplitudes, phase synchronization, and their LRTCs and contribute to the large inter-individual variability therein. We furthermore postulated that these effects could be achieved via modulations of brain criticality. More specifically, scale-free LRTCs are hallmarks of systems with critical or near-critical dynamics, suggesting that the brain operates near a critical phase transition between disorder and order, *i.e.*, between inadequate and excessive synchronization, respectively. Importantly, brain criticality is primarily thought to be controlled by the excitation-inhibition (E/I) ratio so that critical dynamics emerge at balanced E/I while excess of inhibition or excitation leads to sub- or super-critical dynamics, respectively [33, 52, 53]. Here, the E/I balance, or "neuronal gain", indicates the functional net effects of inhibitory and excitatory synaptic, cellular, biophysical, and microcircuit mechanisms at the systems-level [54]. Brains may normally operate in a slightly subcritical regime [55], where LRTCs in human brain activity [31, 32, 35, 36] exhibit large inter-individual variability. We hypothesized that modulations in oscillation dynamics would be obtained via inter-individual differences in the neuromodulation levels, which could result in differences in systems-level net E/I balance (or neural gain). In the brain criticality framework, the carriers of different variants of the *COMT* Val^{158}Met and *BDNF*

138 Val^{66}Met polymorphisms, would therefore be located closer to or further away from the critical
139 point (Fig 1A-B). This would lead to the different genotype cohorts (Fig 1B) showing consistent
140 differences in local amplitudes, global synchronization, and LRTCs (Fig 1C-D, see Fig 1A).
141 Alternatively, *COMT* and especially *BDNF* could induce plastic changes in the structural
142 connectivity networks (SC) [50, 51] which in turn could lead to changes in FC [17]. To test these
143 hypotheses, we measured resting-state brain dynamics with MEG and estimated local oscillation
144 amplitudes, large-scale phase synchronization, and LRTCs from individually source-reconstructed
145 MEG data. We then investigated their correlation with the *COMT* Val^{158}Met and *BDNF* Val^{66}Met
146 polymorphisms estimated from SNP analysis (Fig 1) and compared the results with predictions
147 from computational modeling. In line with the predictions of the brain criticality framework and
148 computational modeling, we found that the *COMT* Val^{158}Met and *BDNF* Val^{66}Met polymorphisms
149 influenced local oscillation amplitudes and LRTCs, and that correlations between oscillation
150 amplitudes and LRTCs were stronger in the polymorphism groups that were located closer to the
151 critical point. The *BDNF* polymorphism contributed also to the strength of large-scale
152 synchronization, but the strongest effects on global synchronization were due to other mechanisms
153 than the shift in the system's E/I balance.
154
155 **Fig 1. A schematic of study outline and rationale.**
156 (A) Computational model of local and inter-areal synchronization dynamics in the realistic human
157 connectome shows that both local (amplitude) and inter-areal synchronization increase
158 monotonically with increasing coupling (control parameter K) and exhibit a phase-transition
159 between low- (subcritical) and high-synchronization (supercritical) regimes. Conversely, the DFA
160 scaling exponent, a measure of long-range temporal correlations (LRTCs), peaks at the critical
161 point. The model predicts that two cohorts (A, B) with subjects operating in different parts of the

subcritical regime should exhibit group differences in amplitude, LRTCs, and inter-areal synchronization. (B) Genotyping of the participants (N = 82) was used to identify the *COMT* Val^{158}Met (rs4680) and *BNDF* Val^{66}Met (rs6265) genetic polymorphisms. (C) MEG data were source-reconstructed using minimum-norm estimation with individual MRI-based head and cortical surface anatomy and filtered to narrowband signals of cortical parcels. Oscillation mean amplitudes and LRTCs were estimated for each parcel and inter-parcel phase synchronization for all parcel pairs. (D) In group analyses, we assessed the anatomical distribution of mean amplitudes, LRTCs, and synchronization within the polymorphism groups and identified statistically significant differences between these groups (Figs 2-4).

Results

COMT Val/Met and *BDNF* Val polymorphisms are associated with the strongest oscillation amplitudes

To characterize local synchronization, we first evaluated mean oscillation amplitudes for 26 wavelet frequencies between 3–60 Hz and averaged the mean amplitudes across 148 cortical parcels separately for participants grouped according to the *COMT* Val^{158}Met (Val/Val, Val/Met, Met/Met) and the *BDNF* Val^{66}Met (Val/Val and the combined Val/Met and Met/Met) polymorphisms. As observed commonly in resting state, oscillation amplitudes peaked in the alpha band (α, 8–14 Hz) (Fig 2A). We then clustered oscillations to frequency bands based on the similarity of the anatomical amplitude maps using Louvain clustering (S1 Fig) that revealed spatial similarity in theta (θ, 3–7 Hz), alpha, beta (β, 14–30 Hz) and gamma (γ, 30–60 Hz) frequency bands. Statistical analysis for these frequency bands using repeated measures ANOVA demonstrated a main effect of frequency [$F(1.86, 150.76) = 98.54$, $p = 6.47\text{E-}27$, $\eta_p^2 = 0.549$] ($N = 82$) on oscillation amplitudes

185 at the whole-brain level. Post-hoc tests indicated that the oscillation amplitudes were stronger in
186 the α band than in the θ ($t(81) = 14.14$, $p = 8.93E-23$), β ($t(81) = 2.75$, $p = 0.043$) and γ ($t(81) =$
187 5.11, $p = 1.3E-5$) bands (t-test, Bonferroni corrected). β-band amplitudes were also stronger than
188 in θ ($t(81) = 15.71$, $p = 1.57E-25$) and γ ($t(81) = 5.49$, $p = 3.0E-6$) bands, and γ amplitudes were
189 stronger than θ band amplitudes ($t(81) = 12.73$, $p = 2.75E-20$). We also showed in these frequency
190 bands that *COMT* Val^{158}Met and *BDNF* Val^{66}Met polymorphisms had no impact on oscillation
191 amplitudes at the whole-brain level (S2 Fig). We further confirmed that oscillation amplitudes were
192 not dependent on the age or gender of the participants (S1 and S2 Tables).
193
194 **Fig 2. *COMT* and *BDNF* polymorphisms influence oscillation amplitudes.**
195 (A) Oscillation amplitudes averaged across parcels for the *COMT* (Val/Val, purple, $n = 18$;
196 Val/Met, turquoise; $n = 48$; and Met/Met, orange, $n = 16$) and *BDNF* polymorphism groups
197 (Val/Val, purple, $n = 66$; Met carriers, orange, $n = 16$). Shaded areas represent 95% bootstrapped
198 confidence intervals of the group means. (B) The fraction P of parcels with a significant positive
199 and negative pairwise difference (shown separately) between the *COMT* and *BDNF* polymorphisms
200 groups in oscillation amplitudes (Mann–Whitney-U test, $p < 0.05$). The light grey area indicates the
201 5% alpha level for findings expected by chance under the null hypothesis and the dark grey area
202 indicates the range (3% total) in fractions of significant parcels observable by chance at $p_q < 0.05$
203 in any single frequency band across the spectrum (26 frequencies). (C) Cortical parcels where the
204 amplitudes differed significantly between polymorphism groups (indicated above the brain
205 surfaces) in the θ (3–7 Hz), β–γ (20–60 Hz), and α to low-β (7–18 Hz) frequency ranges in at least
206 one of the individual frequencies. The color scale indicates the max-normalized amplitude
207 differences for *COMT* (red) and *BDNF* (blue) polymorphisms independently, so that parcels where
208 the effects are co-localized have purple hues. Abbreviations are formed from a combination of i)

Areas: a = anterior, ca= calcarine, d = dorsal, i = inferior, la = lateral, m = middle, mrg = marginal, opc = opercular, p = posterior, s = superior, tr = triangular and ii) Lobes: C= central / cingulate, F= frontal, P= parietal, O= occipital, T=temporal, and iii) Gyrus = G, Sulcus = S. Additional abbreviations subC = subcentral gyrus/sulcus, preCN=precuneus.

To identify possible anatomically limited polymorphism effects, we tested significant pairwise differences between polymorphism groups at the anatomical resolution of individual parcels and for each frequency. For *COMT*, the amplitudes were stronger (Mann-Whitney-U test, $p < 0.05$) for Val/Met heterozygotes than for Met or Val homozygotes in the θ band as well as in the α to low-β bands (7–18 Hz) (in up to 24% and 17% of cortical parcels, respectively) (Fig 2B), whereas opposite effects were observed in the high-β to γ (20–60 Hz) bands (16% for Met, 9% for Val), along with stronger amplitudes in Met compared to Val homozygotes (9%). For *BDNF*, oscillation amplitudes were stronger for the Val homozygotes than for the Met carriers in the θ and in the α to low-β bands (up to 23% of the parcels), whereas a small opposite effect was observed in high-β to γ bands. We next plotted the amplitudes in each cortical parcel separately for each polymorphism group (S3-S4 Figs) and their significant differences (Fig 2C) in the cortical anatomy. Stronger oscillation amplitudes for the *COMT* Val/Met heterozygotes were localized to the central sulcus (CS), anterior, mid- and posterior cingulate cortex (aCC, mCC, pCC), inferior frontal gurys (iFG), right-hemispheric middle frontal gyrus (mFG) and inferior parietal gyrus (iPG), inferior part of the insula (iINS) and precuneus (preCN) (Fig 2C). The parcels were co-localized with fMRI-based functional parcellation (S5 Fig), which revealed that these parcels mostly belonged to the frontoparietal network (FPN) and default mode network (DMN). Of these regions, iPG and left iINS and left CS showed also larger amplitudes for *BDNF* Val homozygotes than for Met carriers. However, the larger amplitudes for *COMT* Met homozygotes compared to Val/Met heterozygotes

in the β-γ bands were localized to superior precentral sulcus (spreCS), corresponding to frontal eye fields (FEF). For *BDNF* Val homozygotes, oscillation amplitudes were larger than in Met carriers in iFS, parieto-occipital sulcus (POS) and postcentral sulcus (poCS) in θ to low-β bands. *COMT* and *BDNF* jointly affected the θ and the α to low-β band oscillation amplitudes in the CS and iPG. In the high-β to γ bands, oscillation amplitudes were stronger for the *COMT* Val or Met homozygotes as compared to Val/Met heterozygotes in preCS, aCC, pCC and the middle frontal gyrus (mFG) and for the *BDNF* Met carries as compared to *BDNF* Val homozygotes in the superior frontal gyrus (sFG) of the left hemisphere and middle temporal gyrus (mTG) of both hemispheres (Fig 2C). However, when amplitudes were averaged within the fMRI-based functional systems, no evident patterns emerged (S5-S6 Figs).

COMT Val^{158}Met and *BDNF* Val^{66}Met polymorphisms influence DFA scaling exponents

We quantified long-range temporal correlations (LRTCs) in oscillation amplitude fluctuations by using detrended fluctuation analysis (DFA) [56] and estimated the mean DFA scaling exponents in all wavelet frequencies (3–60 Hz). To obtain a whole brain view on LRTCs, DFA exponents were first averaged across parcels separately for each *COMT* Val^{158}Met and *BDNF* Val^{66}Met polymorphism group for each frequency (Fig 3A). Statistical analysis for the canonical frequency bands with repeated measures ANOVA showed a main effect of frequency [$F(2.16, 174.70) = 123.65$, $p = 9.85\text{E-}36$, $\eta_p^2 = 0.604$] ($N = 82$). Post-hoc test indicated that DFA exponents in α band were stronger than in θ ($t(81) = 13.00$, $p = 1.00\text{E-}22$), β ($t(81) = 10.00$, p = 1.14E-11) and γ ($t(81) = 12.80$, $p = 3.58\text{E-}21$) bands (t-test, Bonferroni corrected). Similarly, also the β band DFA exponents were stronger than in θ ($t(81) = 10.33$, $p = 5.09\text{E-}14$) and γ ($t(81) = 10.75$, $p = 6.04\text{E-}17$)

bands, and the DFA exponents in θ band were stronger than in γ band ($t(81) = 3.00$, $p = 0.008$). *COMT* polymorphism had an effect on whole-brain DFA exponents in the γ frequency band averaged across the brain and within the canonical frequency band (univariate ANOVA, [$F(2, 75) = 3.80$, $p = .027$, $\eta_p^2 = 0.092$]), when age was controlled for ($n = 79$) (S2 Fig). Group mean exponents were higher at the γ-band for the *COMT* Val/Met individuals than for the Val/Val ($t(64) = 2.08$, $p = 0.043$, uncorrected) and Met/Met ($t(62) = 3.50$, $p = 0.001$) individuals when equal variances were not assumed. The *BDNF* polymorphism affected the whole-brain DFA exponents in the α band [$F(1, 76) = 4.19$, $p = .044$, $\eta_p^2 = .052$] whereby the Val homozygotes exhibited larger LRTC exponents than the Met carriers (Fig 3A and S2).

Fig 3. Influence of *COMT* and *BDNF* polymorphisms on LRTCs. (A) Detrended fluctuation analysis (DFA) exponents averaged across parcels for the *COMT* and *BDNF* polymorphism groups. Shaded areas represent 95% bootstrapped confidence intervals of group means. Black bar with asterisk denotes the range of frequencies with significant differences between the *BDNF* polymorphism groups (Kruskal-Wallis, $p < 0.05$, uncorrected). (B) Fractions (P) of parcels with a significant positive and negative difference between C*OMT* and *BDNF* polymorphism groups in the DFA exponents (Mann–Whitney-U test, $p < 0.05$), as in Fig 2B. (C) Cortical areas where significant differences between polymorphism groups in the DFA exponents were found in the θ, β–γ and α–β -bands (Mann–Whitney U test, $p < 0.05$, corrected). Colors and abbreviations as in Fig 2C.

Similar to oscillation amplitudes, *COMT* Val^{158}Met and *BDNF* Val^{66}Met polymorphisms had a more robust effect on the DFA exponents at the resolution of cortical parcels indicating large anatomical heterogeneity. DFA exponents were greater for the *COMT* Val/Met heterozygotes than

for the *COMT* Met homozygotes (Mann-Whitney-U test, $p < 0.05$) in the θ band (up to 35% of parcels) and in the β–γ band (up to 60%) (Fig 3B). Further, θ band DFA exponents were greater for Val/Val than for Met/Met (18%) and β–γ DFA exponents were greater in Val/Met than for Val/Val (49%) (Fig 3B). For *BDNF,* a robust effect of polymorphism was found for DFA exponents. These were greater for Val homozygotes than Met carriers in the θ band (57%) and in α- low-β bands (83%) (Fig 3B). The effect of *COMT* Val^{158}Met and *BDNF* Val^{66}Met on DFA exponents was thus more extensive compared to that found for oscillation amplitudes. The localization of DFA exponents for each polymorphism group (S7-S8 Figs), and their significant differences (Fig 3C) revealed wide-spread group differences. In the θ band, large differences between *COMT* Val/Met heterozygotes and Met homozygotes and between *BDNF* Val homozygotes and Met carriers were co-localized to preCS, mCC, and mFG (Fig 3C). DFA exponents in θ band were also greater for *COMT* Val/Met group in INS, pCC, and in β–γ band particularly in parcels of the somatomotor (SM) network, and DMN. *BDNF* Val homozygotes had greater α–low-β band LRTC exponents than Met carriers nearly in all parcels of the cortex (Fig 3C). Co-localization with fMRI-based functional parcellations reproduced these findings, but again revealed no evident patterns in the localization (S9 Fig).

Finally, to gain insight for the common effects of *COMT* Val^{158}Met and *BDNF* Val^{66}Met polymorphisms on oscillation amplitudes and DFA exponents, we co-localized their effects. This revealed co-localization in the parcels of PFC and PPC, CS and anterior cingulate structures (S10 Fig). The effects of *COMT* and *BDNF* polymorphisms on LRCTs were widespread, in line with prior work and with the idea that LRTCs reflect global fluctuations in neuronal activity across the brain's modular structure [13, 29, 35].

BDNF polymorphism correlates with the strength of large-scale phase-synchronization

To obtain a global view on the influence of *COMT* Val^{158}Met and *BDNF* Val^{66}Met polymorphisms on neuronal dynamics, we estimated their impact on inter-areal phase coupling of neuronal oscillations a.k.a. synchronization that constitutes a key characteristic of individual cortical dynamics and has fundamental influence on behavior [1, 3, 4, 7, 11, 16]. We estimated phase-synchrony among all cortical parcels with the weighted phase-lag index (wPLI) that is less sensitive to linear source mixing [57] and computed the mean synchronization for each of the *COMT* Val^{158}Met and *BDNF* Val^{66}Met polymorphism group (Fig 4A). At the whole brain level, the mean phase-synchronization varied between the canonical frequency bands as indexed by a main effect of frequency in a repeated measures ANOVA [$F(1.69, 136.53) = 18.29$, $p = 5.45E\text{-}7$, $\eta_p^2 = .184$] ($N = 82$, S2 Fig). Synchronization was stronger in the α band compared to θ ($t(81) = 3.00$, $p = 2.12E\text{-}4$) and β bands ($t(81) = 13.04$, $p = 3.14E\text{-}20$), while mean synchrony did not differ between α and γ, and θ and γ bands (t-test, Bonferroni corrected). Synchronization was overall weakest in the β band as compared with θ ($t(81) = 7.54$, $p = 7.09E\text{-}11$), α and γ ($t(81) = 3.00$, $p = 0.004$) bands.

Fig 4. *BDNF* polymorphisms influence large-scale phase-synchronization. (A) Phase-synchronization averaged across the whole brain for the *COMT* Val^{158}Met and *BDNF* Val^{66}Met polymorphism groups with 95% bootstrapped confidence intervals. Black bars with asterisks denote the frequencies where a significant group difference was found (Kruskal-Wallis, $p < 0.05$, uncorrected). (B) The differences in the phase synchrony (Δ-wPLI) within and between functional systems for the *BDNF* Val homozygotes and Met carries, averaged across hemispheres and wavelet

326 frequencies in these frequency bands. Color indicates Δ-wPLI, red indicating stronger
327 synchronization for *BDNF* Val^{66} homozygotes and blue for Met carriers. Stars denote the brain
328 system pairs where the group difference was significant (Kruskal-Wallis, *: $p < 0.05$, uncorrected,
329 **: $p < 0.05$, Benjamini-Hochberg corrected). Abbreviations: DAN = Dorsal attention network,
330 DMN = Default Mode network, FPN = Frontoparietal network, Lim = Limbic system, SM=
331 Somatomotor network, Vis = Visual network, VAN = Ventral attention network.
332
333 We did not find significant differences (Kruskal-Wallis test, $p < 0.05$) among the *COMT*
334 Val^{158}Met polymorphism groups, but the mean synchronization for *BDNF* Val homozygotes was
335 stronger than for *BDNF* Met carriers in the θ and α frequencies (Fig 4A). To acquire
336 neuroanatomical insight into the patterns of inter-areal synchronization in functional brain systems,
337 we collapsed the parcel-wise synchronization estimates within brain systems defined by fMRI
338 functional connectivity [58] and for the same frequency bands that were used for estimating
339 oscillation amplitudes and LRTCs (S1 Fig). Corroborating the mean-synchronization result,
340 synchronization between or within the subsystems did not differ significantly among the *COMT*
341 Val^{158}Met polymorphisms (absolute values in S11 Fig). However, *BDNF* Val homozygotes
342 exhibited stronger synchronization than Met carriers in the α band between and within nearly all
343 subsystems (Fig 4B and S11 Fig, Kruskal-Wallis test, $p < 0.05$, corrected with Benjamini-
344 Hochberg). We also computed synchronization separately for each hemisphere and between the
345 hemispheres. Interestingly, synchronization in the α and β bands was more robust for the left- and
346 inter-hemispheric connections than for the right-hemispheric connections (S12 Fig). Additionally,
347 β-band synchronization was stronger for *BDNF* Val homozygotes than Met carriers in the left-
348 hemispheric attentional networks including FPN, dorsal attention network (DAN), ventral attention
349 (VAN) and Limbic networks (Lim) and DMN.

Computational model-based approach to neuromodulation effects on critical synchronization dynamics.

We hypothesized that at the level of macroscopic brain dynamics, the effects of *COMT* Val^{158}Met and *BDNF* Val^{66}Met polymorphisms, could be addressed in the context of brain criticality if these polymorphisms bias the underlying "control parameter" that tunes the distance of neuronal systems to criticality. To assess the relationships of the observable brain dynamics measures with the control parameter, we used a computational model of synchronization dynamics exhibiting a transition from sub- to super-critical dynamics. We implemented a nested Kuramoto model with separable local network (cortical parcel) and large-scale (whole-brain network) levels [12]. Synchronization here was regulated by local and global coupling parameters that simulate the E/I balance (or neural gain) that is the likely primary control parameter for brain criticality [52, 59]. In the model, increasing coupling led to parallel strengthening of local amplitudes, large-scale synchronization, and LRTCs throughout the subcritical regime up to the critical point (Fig 1A). We used modelling to predict the synchronization dynamics of neuronal oscillations for two hypothetical cohorts (A and B) operating in a subcritical regime. The model predicted that the cohort (B), operating at greater excitability / gain, exhibited greater oscillation amplitudes, LRTCs, and large-scale synchronization (Fig 1A, Fig 5A), and as a novel model-predicted measure, their mutual correlations (Fig 5B). To investigate whether *COMT* and *BDNF* polymorphism could influence synchronization dynamics via these mechanisms, we computed these dynamics separately for different polymorphism groups. In line with the model predictions, the *BDNF* Val/Val (Fig 5C) and *COMT* Val/Met (Fig 5D) groups were associated with significantly elevated amplitudes and LRTCs compared to the other polymorphisms. The *BDNF* Val/Val group also showed stronger global synchronization (Fig 5C). Further, local correlations between amplitude and criticality in the

374 θ band were stronger among the *BDNF* Val/Val and *COMT* Val/Met groups (Fig 5 E-F) and in the
375 γ bands for *BDNF* (S13 Fig). While there were no group differences in the correlation between
376 global inter-areal synchronization and criticality in the α band (Fig 5E) where the *BDNF*
377 polymorphism effects were the strongest, the group differences were in line with the model
378 predictions in the θ band, in which the influence of *BNDF* polymorphism on global synchronization
379 was weaker. These findings thus provide converging evidence that locally, *COMT* Val^{158}Met and
380 *BDNF* Val^{66}Met polymorphisms impact oscillation dynamics as predicted by the framework of
381 brain criticality under the hypothesis that these polymorphisms influence the control parameter of
382 cortical critical dynamics. In contrast, the most robust effects of *BDNF* on large-scale
383 synchronization were not in line of the model predictions, suggesting that these were mediated by
384 other factors than the control parameter of brain criticality.
385
386 **Fig 5. Model and experimental evidence for modulation of brain criticality.** (A) Local
387 amplitude (A), inter-areal phase synchronization (PLV), and DFA exponents in modeled data for
388 two cohorts A (orange) and B (purple). All metrics are greater for the cohort B that is designed to
389 operate closer to the critical point (see Fig 1) than cohort A. The box ends indicate the lower quartile
390 (Q1, 25th percentile) and upper quartile (Q3, 75th percentile) across cortical regions/parcels,
391 notches indicate the median, and whiskers indicate the range of Q1 – 1.5 * IQR and Q3 + 1.5 *
392 IQR, where IQR is the inter-quartile range (Q3-Q1). (B) Correlations between amplitude and DFA
393 exponents, and between PLV and DFA, in modeled data are also larger for cohort B than the more
394 subcritical cohort A. (C) A and DFA exponents in θ band, and global phase synchronization (wPLI)
395 in α band for the *BDNF* Val homozygotes (purple) and Met carriers (orange) in MEG data. (D) A
396 and DFA exponents for *COMT* Val^{158}Met polymorphism groups in the θ band. (E) Correlation
397 between A and DFA exponents differs between *BDNF* Val^{66}Met polymorphism groups in the θ-

band, as does the correlation between wPLI and DFA exponents in θ but not in α band. (F) Correlation between A and DFA exponents in θ band differs between *COMT* Val^{158}Met polymorphism groups.

Discussion

Inter-individual variability in spontaneous brain dynamics shapes human behavioral performance and cognitive ability [4, 12, 16, 60, 61]. While the causes of this variability are diverse, genetics influences numerous factors that are important for brain oscillation dynamics on multiple scales observed in human MEG and EEG data [37, 39, 40]. Cellular level influence of macroscopic oscillations can be achieved through regulation of neural circuits and dynamic circuit motifs [2, 37, 39] as well as coupling of metabolic activity and connectivity [15]. However, it is not well understood how the genetic biases of molecular, cellular, and micro-circuit mechanisms translate into alterations of macroscopic brain dynamics that are observable in electrophysiological neuroimaging. We tested here the hypothesis that the *COMT* Val^{158}Met and *BDNF* Val^{66}Met genetic polymorphisms contribute to the variability in emergent local (oscillation amplitudes and LRTCs) and global (inter-areal phase synchronization) dynamics of neuronal oscillations via their regulation of the neuromodulators dopamine (DA), norepinephrine (NE), and serotonin (5-HT). We showed that, indeed, both *COMT* and *BDNF* polymorphisms influenced oscillation amplitudes and LRTCs, while the *BDNF* polymorphism also impacted the strength of global synchronization.

Local oscillation strength and dynamics are modulated by genetic polymorphism in *COMT* and *BDNF*

The amplitude of θ oscillations was greater for *COMT* Val/Met heterozygotes than for *COMT* Val or Met homozygotes, and the amplitudes of θ and α oscillations were greater for *BDNF* Val homozygotes than for Met carriers. These data thus add to scarce prior observations about *COMT* polymorphism effects on electrophysiological activity [62-64], which have shown using EEG sensor level analysis that *COMT* Val homozygotes had lower individual α power in both waking state and sleep than Met homozygotes [63] and that the *COMT* polymorphism influences phase-resetting of γ oscillatory activity in attention [64]. Our results provide strong evidence for *COMT* polymorphism influencing local amplitude dynamics in widespread brain areas. We furthermore found the *BDNF* Val homozygotes to exhibit stronger α band amplitudes bilaterally in frontoparietal regions and parcels of the visual system in line with previous research [65] and that 5-HT plays a critical role in modulating cortical activity and neuronal oscillations [66, 67].

To our knowledge, this study is the first to report the influence of genetic polymorphism on LRTCs in oscillation amplitude fluctuations. LRTCs were stronger for the *COMT* Val/Met heterozygotes than for Val or Met homozygotes and stronger for *BDNF* Val homozygotes than for Met carriers, demonstrating that near-critical dynamics of brain oscillations is influenced by *COMT* and *BDNF* polymorphisms. The temporally widespread effects of *COMT* and *BDNF* polymorphisms on both instantaneous amplitudes and their LRTCs could putatively stem from *COMT* influencing both phasic and tonic firing modes of DA neuronal spiking [68] and/or from multi-scale cortical ensemble codes by NE [69].

The finding of the strongest amplitudes and LRTCs in the *COMT* Val/Met polymorphism group, is consistent with previous findings showing that the impact of neuromodulation on

442 cognition follows an "inverted-U-shaped" function, where both too little and too much
443 neuromodulation impairs performance [20, 47, 70-72]. The association between *COMT* Val^{158}Met
444 polymorphism and neuronal activity has been frequently observed in fMRI to be predominantly
445 localized to PFC, which has low DA reuptake and higher COMT levels. In our data, the influence
446 of *COMT* Val^{158}Met polymorphism on instantaneous amplitudes was not localized specifically to
447 PFC, but to multiple specific cortical regions in the FPN and cingulo-opercular (CO) networks.
448 These networks underlie the dual control of executive functions [73] and have been shown to be
449 functionally coupled also in the resting state [74] which is in agreement with the role of DA in
450 cognitive control [70, 75]. Further, our results are in line with brain-wide distribution of
451 catecholamine-induced changes in DA and NE in intrinsic fMRI correlations [21] and with findings
452 that DA innervation covers the entire cortex [76] and Locus Coeruleus' NE projections reach a
453 variety of targets [69]. Overall, these results support the idea that via DA and NE *COMT* influences
454 local oscillation dynamics in a variety of cortical regions important for cognition.
455

456 Polymorphism in *BDNF* but not in *COMT* influences inter-areal
457 synchronization dynamics

458 The influence of *BDNF* and *COMT* polymorphisms on large-scale synchronization
459 networks have this far remained uncharted. We found that *BDNF* Val^{66}Met polymorphism
460 influenced large-scale global inter-areal phase synchronization. This effect was robust in the α
461 band, in which stronger synchronization was observed for *BDNF* Val homozygotes in all functional
462 subsystems except within the visual system. *BDNF* Val homozygotes also had stronger β band
463 synchronization between the frontoparietal attention networks and DMN, and stronger θ
464 synchronization between DAN and SM networks, but only in the left hemisphere. This robust

465 modulation of synchronization dynamics by *BDNF* polymorphism could contribute to significant
466 differences across individuals in behavior and cognition, which have been shown to be strongly
467 influenced by spatial and spectral characteristics of oscillatory synchronization [12, 14, 17].

468 However, large-scale synchronization was not influenced by *COMT* Val^{158}Met
469 polymorphism. This suggests that catecholaminergic neuromodulatory drive does not play a
470 significant role in instantaneous resting-state network synchronization even though it modulates
471 local oscillatory dynamics in both sub-second and seconds-to-minutes timescales. This finding
472 differs from prior results which have found catecholamines to be related to fMRI-based changes in
473 functional connectivity by using catecholamine blocker atomoxetine [21]. These differences might
474 be explained by different effects of catecholaminergic levels on BOLD signal and
475 electrophysiological connectivity or by *COMT* polymorphism having more subtle effects on
476 neuronal dynamics compared to neuropharmacological interventions.

477

478 Computational modelling predicts local influences to depend on net 479 excitability

480 Near-critical synchronization dynamics has been proposed as a fundamental operating
481 principle of brain functioning, enabling transient and flexible computations that are beneficial for
482 the individual by maximizing information storage and transmission [60, 77-81]. This notion has
483 been supported experimentally by behavioral data [82] and *in vitro* studies [52]. Here we show that
484 genetic polymorphism in *COMT* and *BDNF* influenced the individual near-critical synchronization
485 dynamics and proximity to the critical point.

486 The systems-level E/I ratio (or gain) is thought to be the primary control parameter for the
487 regulation of critical brain dynamics [52, 59], and to influence brain dynamics using whole-brain
488 modeling [83]. We postulated that the observed differences in neuronal synchronization dynamics

are due to neuromodulation-related shifts in the system's net E/I ratio and/or gain. Comparison of the experimental and computational-model data showed that the *COMT* Val^{158}Met and *BDNF* Val^{66}Met polymorphisms influenced local oscillatory dynamics and their correlations in line with the brain criticality framework. More specifically, *COMT* Val^{158}Met heterozygotes and *BDNF* Val^{66} homozygotes had greater values of and correlations between LRTCs and oscillation amplitudes than the other polymorphism groups, indicating that they are associated with a higher value of the underlying control parameter, *i.e.*, with greater net excitatory drive or neuronal gain [28] compared to *COMT*^{158} homozygotes and *BDNF*^{66} Met carriers. This is in accordance with the framework in which neuromodulatory drive influence brain-state energy landscape facilitating with transitions in the whole-brain neural states [84, 85].

In contrast, large-scale synchronization that was influenced by *BDNF* Val^{66}Met polymorphism, was modulated only partially in line with the model predictions. Global α-band synchronization that was robustly modulated by the *BDNF* Val^{66}Met polymorphism, was correlated with LRTCs according to the model predictions, but there were no differences between polymorphism groups. This finding implies that the strongest effects of *BDNF* polymorphisms on global synchronization are not due to a shift in the system's excitation, but to other mechanisms such as the influence of BDNF on maintenance, maturation, and formation of neuronal networks [50, 51] putatively via receptor TrkB (neurotrophic receptor tyrosine kinase 2) signaling [86, 87]. These could impact large-scale network synchronization via changes in structural connectivity [17]. Yet, the weaker effect of *BDNF* polymorphism on θ and β band synchronization was congruent with changes in the model's control parameter, suggesting that these global synchronization patterns might be strengthened also by increased excitatory drive for the *BDNF* Val^{66} homozygotes. This finding is in agreement with computational modeling results showing that the dynamic connectome is explained by dynamical mutual coupling between 5-HT neurotransmitter systems

513 [19]. Thus, *BDNF* seems to influence critical synchronization dynamics both via modulations in
514 the brain serotonin levels leading to changes in the neuronal gain as well as via other mechanisms
515 influencing the formation and survival of neuronal networks.
516

517 # Conclusions

518 Our data showed that the *COMT* Val^{158}Met and *BDNF* Val^{66}Met polymorphisms contribute
519 to the variability of oscillation dynamics. In addition to *COMT* and *BDNF*, many other genetic
520 factors are likely to contribute to these oscillation dynamics, as observed for the cortical structure
521 [88]. *COMT* Val^{158}Met and *BDNF* Val^{66}Met polymorphisms influenced local oscillatory dynamics
522 putatively via modulations in the neuromodulator levels leading to changes in net excitatory drive
523 or gain in the neuronal networks. At the synaptic level, DA, NE, and 5HT could influence E/I ratio
524 and gain control via various cellular, biophysical, and network mechanisms, including their
525 temporal aspects. Taken that this study did not use neuropharmacological interventions, the specific
526 mechanisms by which *COMT* and *BDNF* genetic polymorphisms influence critical oscillation
527 dynamics are beyond of the scope of this study.

528 Because oscillation amplitude fluctuations, LRTCs, and global synchronization dynamics
529 are predictive of behavioral variability over both long [35, 36] and sub-second time scales [4],
530 *COMT* Val^{158}Met and *BDNF* Val^{66}Met polymorphisms may underlie individual differences in trait-
531 like behavior and cognitive performance via their effect on critical oscillatory dynamics and
532 synchronization. Differences in these dynamics caused by genetic polymorphism are likely to
533 influence individuals' cognitive and mental development and may predispose them to specific brain
534 diseases. In line with the latter idea, alterations in the brain E/I ratio have been suggested to
535 predispose individuals to dementia and Alzheimer's disease [89]. Our results thus point in new

536 directions for the investigation of how genetic factors could translate to behavioral variability via
537 modulations of the systems-level neuronal dynamics.
538

539 Materials and methods

540 Experimental Design

541 Resting-state brain activity was recorded from healthy volunteers (N = 82, 18–55 years of
542 age; mean age: 29 years; 6 left-handed; 44 female) with 306-channel MEG (Vectorview, Elekta-
543 Neuromag, LtD) at a sampling rate of 600 Hz. The subjects fixated on a central fixation cross
544 throughout the ~8 min resting-state MEG-recording (duration 7.8 ± 2.9 min, mean ± standard
545 deviation, S1 and S2 Tables). Blood samples for the collection of DNA were obtained before each
546 MEG session. T1-weighted anatomical magnetic resonance imaging (MRI) MP-RAGE scans were
547 obtained for each participant at a resolution of 1 × 1 × 1 mm using a 1.5 T MRI scanner (Siemens,
548 Germany) on a separate day. The dataset collected for this study is part of a broader project
549 "Tunteet" that includes also other datasets and paradigms. The study was performed in accordance
550 with the Declaration of Helsinki and with permission of the Ethical Committee of the Helsinki
551 University Central Hospital. All participants gave a written informed consent prior to the
552 recordings.
553

554 Genotyping

555 DNA was extracted from blood samples according to standard procedures at the National
556 Institute for Health and Welfare. DNA samples were genotyped at Estonian Genome Center using
557 Infinium PsychArray-24 v1.1 (Illumina). Quality control (QC) was performed with PLINK 1.9
558 (www.cog-genomics.org/plink/1.9/) [90]. Markers were removed for missingness (> 5%) and

Hardy-Weinberg equilibrium ($p < 1 \times 10^{-6}$). Individuals were checked for missing genotypes (> 5%), relatedness (identical by descent calculation, PI_HAT > 0.2) and population stratification (multidimensional scaling). Our sample for the *COMT* gene consisted of 18 Val/Val, 48 Val/Met, and 16 Met/Met individuals (S1 Table). A one-way ANOVA confirmed that the *COMT* polymorphism groups did not differ in terms of age [$F(2, 46) = 0.05$, $p = .984$] and the duration of the resting state recording [$F(2, 46) = 0.32$, $p = .726$]. A chi-square test further confirmed that the percentages of female and male participants did not differ between the *COMT* polymorphism groups [$X^2(2) = 2.11$, $p = .349$]. The *BDNF* sample consisted of 66 Val/Val, 14 Val/Met, and 2 Met/Met individuals (S2 Table). As the Met/Met polymorphism had a low frequency, we combined Met carriers (*i.e.,* Val/Met and Met/Met polymorphisms) into one group [see also 91]. An independent samples *t*-test (2-tailed) confirmed that the *BDNF* polymorphisms did not differ in terms of age [$t(32) = 0.20$, $p = .847$] or the length of the resting state recording [$t(32) = 0.76$, $p = .444$]. A chi-square test showed no differences in the percentages of female and male participants between the *BDNF* polymorphisms [$X^2(1) = 0.00$, $p = .995$].

Preprocessing and filtering of MEG data

Signal space separation method (tSSS) [92] with the Maxfilter software (Elekta Neuromag, Helsinki, Finland) was used first to suppress extracranial noise, interpolate bad channels and to co-localize the recordings in signal space individually for each participant. Next, independent component analysis (ICA, Matlab toolbox Fieldtrip [93] was used to extract and exclude signal components that were correlated with eye movement, blink and cardiac artifacts. The preprocessed MEG data were filtered into 26 logarithmically spaced frequency bands, $f_{min} = 3$ Hz; $f_{max} = 60$ Hz using complex Morlet Wavelets

583 $$w(t, f_0),\ w(t, f_0) = A\exp(-t^2/2\sigma_t^2\ 2)\exp(2i\pi f_0 t),$$

584

585 where $\sigma_t = m/2\pi f_0$, i is the imaginary unit, m (=5) defines the compromise between time and
586 frequency resolution, and f_0 is the center frequency. After filtering, the time-series data were
587 decimated to a frequency-dependent sampling rate of between 2 and 5 times the center frequency.

588

589 ## Source Analysis and Surface Parcellations

590 Volumetric segmentation of the MRI data, surface reconstruction, flattening, cortical
591 parcellations and neuroanatomical labeling with the Freesurfer/Destrieux atlas [94] were performed
592 using FreeSurfer software (http://surfer.nmr.mgh.harvard.edu/). Single-layer boundary element
593 conductivity models and cortically constrained source models for the MEG-MRI co-localization
594 and the preparation of the forward and inverse operators [95] were carried out using minimum norm
595 estimate with MNE software (https://mne.tools/stable/index.html) [96]. Noise covariance matrices
596 (NCMs) were computed using preprocessed broad-band filtered (125–195 Hz, with 150 Hz notch)
597 MEG time series around synthetic resting state events that were spaced in every 1 seconds and then
598 used to compute minimum-norm estimate (MNE) inverse operators for all wavelet frequencies.
599 These inverse operators were used to project the sensor-space data into source-space. The source
600 models had dipole orientations fixed to the pial surface normal and a 5 mm inter-dipole separation
601 through the cortex, which yielded models containing 5000–8000 source vertices per hemisphere.
602 As in previous studies [12, 97], source-vertex time-series were then collapsed into parcel time series
603 with an individually source-reconstruction-accuracy- (fidelity-) optimized collapse operators. We
604 used a 400-parcel parcellation that was obtained by iteratively splitting the largest parcels of the
605 Destrieux atlas (148 parcels) [94] along their most elongated axis using the same parcel-wise splits
606 for all participants. Parcels were also assigned to functional systems based on Yeo's 7-parcel

scheme derived from fMRI-connectivity [58]. To control for source-reconstruction accuracy, we estimated *parcel fidelity* as a measure of source-reconstruction accuracy [97].

Estimation of oscillation amplitudes and long-range temporal correlations

The parcel-wise narrow-band filtered time-series were used for cortex-wide mapping of induced oscillation amplitudes (A), LRTCs in oscillation amplitude envelopes, as well as for mapping cortex-wide phase-synchronization networks. Data were averaged for each cortical parcel and frequency separately for subjects in each *COMT* and *BDNF* polymorphisms group. The LRTC exponents of the amplitude envelopes were quantified with detrended fluctuation analysis (DFA) [56].

DFA was applied in two stages. First, time series $X(k)$ were normalized to zero mean and the cumulative sum of the signal was computed:

$$y(k) = \sum_{i=1}^{k} [X(i) - \langle X \rangle]$$

The integrated signal $y(k)$ was then segmented into multiple time windows Δt from 1 to 100 s with minimum window length of 20 cycles and maximum of 100 (length multiplier 1.2) [31]. Second, each segment of integrated data was locally fitted to a linear function $y_{\Delta t}(k)$ and the mean-squared residual $F(\Delta t)$ was computed:

$$\sqrt{\frac{1}{N} \sum_{k=1}^{N} [y(k) - y_{\Delta t}(k)]^2}$$

where N is the total number of data points.

The power law scaling exponent β was defined as the slope of linear regression of the function $F(\Delta t)$ plotted in log–log coordinates, estimated using a least-squares algorithm. The scaling exponent β can be considered a measure of temporal clustering so that $0.5 < \beta < 1.0$ indicates power-law scaling behavior and the presence of temporal correlations, whereas values around 0.5 indicate uncorrelated noise.

Analysis of inter-areal synchronization

To estimate cortex-wide synchronization connectomes, we computed for each subject and for each frequency, phase synchronization between all 400 parcels (or parcels within the left or right hemisphere) using the weighted phase-lag index (wPLI) [98] which is defined as

$$wPLI_{a,b} = \frac{|E\{im(X_{ab})\}|}{E\{|im(X_{ab})|\}} = \frac{|E\{|im(X_{ab})|sign(im(X_{ab}))\}|}{E\{|im(X_{ab})|\}}$$

where im (X_{ab}) is the imaginary part of the cross-spectrum of the complex narrowband time series Z_a and Z_b, and $E\{\ \}$ is the expectancy value operator. The cross-spectrum X_{ab} can be substituted with $= Z_a Z_b^*$, where * denotes the complex conjugate, and the mean over samples can be taken as the expectancy value [12]. The wPLI is insensitive to artificial connections arising as direct effects of zero-phase lagged linear signal mixing that is a major issue in connectivity analysis using MEG/EEG data [4]. Spurious interactions, however, remain as 2nd order effects even when using zero-phase lag insensitive connectivity metrics. Since spurious connections are more likely to be reported for regions with low source-reconstruction accuracy, we removed from the analysis parcels with *fidelity* < 0.2, which led to the exclusion of 9.27%, of possible parcel pairs [12, 97].

Graph theory [99] was used to characterize the network structures in group-level adjacency matrices. Each thresholded adjacency matrix defined a graph made up of nodes and edges, where nodes are cortical parcels and edges are the significant interactions between nodes. The mean

connection strengths were obtained by averaging the strength of all valid edges in the connectome for each subject and then over subjects in each *COMT* and *BDNF* polymorphism group. For functional subsystem analysis, all pairwise interactions were averaged across the frequency bands defined by clustering analyses (S1 Fig) and then collapsed into the 7 functional systems of the Yeo parcellation [58].

Computational modelling

We used a nested Kuramoto model [12] to investigate the covariance and mutual correlations of local synchronization (node/parcel amplitude), inter-areal synchronization, and local LRTCs in a heuristic model of synchronization dynamics. The model was adapted from a conventional Kuramoto model so that it comprised 100 nodes (corresponding to 100 cortical parcels) and each node was modelled by a Kuramoto model of 500 oscillators. The model was defined so that for each node k, the temporal evolution of the phase θ of each oscillator i was described by:

$$\frac{d\theta_i^k}{dt} = \omega_i + \frac{K}{N_{osc.}} \sum_{j=1}^{N_{osc.}} sin(\theta_j - \theta_i) + \sum_{l=1}^{N_{nodes}} W_{k,l} * sin(\varphi_l - \theta_i) + N(0, \sigma)$$

where ω_i is the oscillation frequency of an oscillator, K is the local coupling (control) parameter, φ_l is the average phase of the node l, $W_{k,j}$ is the connection strength between the node k and other nodes j, and $N(0, \sigma)$ is Gaussian noise. For the connection strengths W, we used the log-scaled structural connectome of fiber counts based on the Schaefer parcellation with 100 parcels [100] multiplied by a global coupling (control) parameter L at $L = 0.5$.

Node time series mimicking the parcel time series in MEG data were obtained by averaging the complex time series of the oscillators in the node. Local synchronization was measured by the absolute value of the complex node time series (Kuramoto order) that is comparable to the

amplitude of MEG parcel time series. Phase Locking Value (PLV) was used to measure the pairwise synchrony between nodes and, as in MEG data, the LRTCs we quantified with DFA. We estimated the correlation between amplitudes and DFA exponents, and between synchronization and DFA exponents, across all nodes, by using Spearman's correlation coefficient.

Statistical analysis

Before statistical testing, time-series were collapsed into the 148 parcels of the original Destrieux atlas [94] to limit the number of comparisons and to improve statistical stability by averaging out anatomical variability, which is large across individuals. Group-level upper and lower confidence limits (2.5% and 97.5%) were computed for each polymorphism group with a bootstrapping approach, using $N = 1000$ resamplings with replacement of the subjects in the group. We first used a nonparametric Kruskal-Wallis test ($p < 0.05$) to examine whether amplitudes and DFA averaged across all parcels within each Morlet frequency were significantly different between any of the polymorphism groups (Fig 2A, 3A). We then tested pair-wise differences between the polymorphism groups separately for each parcel and wavelet frequency using the Mann–Whitney U-test ($p < 0.05$) with multiple comparisons initially accounted for with false discovery reduction (FDR) by discarding as many least-significant observations as were predicted to be false by the alpha-level (5% at $\alpha = 0.05$) for each time-frequency bin. We further estimated a threshold (see dark grey area in Figs. 2B and 3B) for the residual fraction of significants so that the probability, p_q, for finding a fraction of significant value above this threshold by chance in any single frequency out of all wavelet frequencies is $p_q < 0.05$.

To test the *COMT* and *BDN*F polymorphism effects on A and DFA on canonical frequency bands, we first estimated spatial similarity across frequency-bands separately for oscillation amplitudes and DFA exponents using machine learning by Louvain community detection [101]

with gamma value of 1.09. This analysis identified canonical frequency bands of theta (θ, 3–7 Hz), alpha (α, 8–14 Hz), beta (β, 14–30 Hz), and gamma (γ, 30–60 Hz) (S1 Fig). We used repeated-measures analysis of variance (ANOVA) (IBM SPSS Statistics) and univariate ANOVA for testing differences in the induced oscillation amplitudes (A), LRTC exponents (β) and inter-areal synchronization (weighted phase-lag index, wPLI) averaged across all parcels between the frequency-bands and between the polymorphism groups respectively. Post-hoc comparisons between group means were made using a *t* test (two-tailed). Multiple comparisons were corrected with Bonferroni correction. The *p* values were also corrected according to the Greenhouse-Geisser procedure when the sphericity assumption was violated. Partial eta squared (η_p^2) is reported as a measure of effect size.

For inter-areal synchronization, confidence intervals were computed with a bootstrapping approach (N = 1000). We tested, for each frequency, whether there was a significant difference between polymorphism groups with a nonparametric Kruskal-Wallis test ($p < 0.05$) and then used the Benjamini-Hochberg method to correct for multiple comparisons. Connection density (K) of the mean connection strengths was used to index the proportion of significant edges from all possible interactions. Differences within and between subsystem connectivity's between the polymorphism groups were then tested for statistical significance with the Kruskal-Wallis test ($p <$ 0.05) and corrected for multiple comparisons with Benjamini-Hochberg (Fig 4A-C).

Finally, we estimated the correlation coefficient between amplitudes and LTRC exponents and between synchronization and LRTC exponents, for each parcel and wavelet frequency across subjects, within the polymorphism groups using Spearman's rank correlation test. Values were then averaged across all parcels and within frequency bands. Confidence limits from 2.5% to 97.5% were obtained from bootstrapping (N = 1000) as above. Significance testing for difference between polymorphism groups was done with permutation statistics (N = 1000) where the subjects were

721 randomly assigned, without replacement, to original-sized polymorphism groups. A difference
722 between groups was considered significant if it exceeded that of 95% of the permutations.
723

724 Competing interests

725 Authors declare that they have no competing interests.
726

727 Data availability

728 Ethical restrictions apply to data and original data cannot be shared on a public server. Data
729 underlying figures, statistics, and main conclusions will be uploaded to Dryad server
730 (https://doi.org/10.5061/dryad.3n5tb2rjp) upon acceptance. All original code has been deposited at
731 https://github.com/palvalab/RS-Gen and is publicly available as of the date of publication.
732

733 References

734 1. Fries P. Rhythms for cognition: Communication through coherence. Neuron. 2015;88:220-
735 35. doi: http://dx.doi.org/10.1016/j.neuron.2015.09.034.
736 2. Womelsdorf T, Valiante, Taufik A , Sahin NT, Miller KJ, Tiesinga P. Dynamic circuit
737 motifs underlying rhythmic gain control, gating and integration. Nature Neuroscience.
738 2014;17(8):1031-9. doi: 10.1038/nn.3764.
739 3. Singer W. Neuronal synchrony: a versatile code for the definition of relations? Neuron.
740 1999;24:49-65.
741 4. Palva S, Palva JM. Discovering oscillatory interaction networks with M/EEG: challenges
742 and breakthroughs. Trends in Cognitive Sciences. 2012;16(4):219-30. doi:
743 10.1016/j.tics.2012.02.004
744 5. Thut G, Miniussi C, Gross J. The functional importance of rhythmic activity in the brain.
745 Current Biology. 2012;22(16):R658-R63. doi: 10.1016/j.cub.2012.06.061.
746 6. Klimesch W, Sauseng P, Hanslmayr S. EEG alpha oscillations: The inhibition–timing
747 hypothesis. Brain research reviews. 2007;51(1):63-88. doi:
748 10.1016/j.brainresrev.2006.06.003.
749 7. Fell J, Axmacher N. The role of phase synchronization in memory processes. Nature reviews
750 neuroscience. 2011;12(2):105-18. doi: 10.1038/nrn2979.
751 8. Siegel M, Donner TH, Engel AK. Spectral fingerprints of large-scale neuronal interactions.
752 Nature Reviews Neuroscience. 2012;13:121-34. doi: 10.1038/nrn3137.

9. Hipp JF, Siegel M. BOLD fMRI correlation reflects frequency-specific neuronal correlation. Current Biology. 2015;25:1368-74. doi: http://dx.doi.org/10.1016/j.cub.2015.03.049.
10. Marzetti L, Della Penna S, Snyder AZ, Pizzella V, Nolte G, de Pasquale F, et al. Frequency specific interactions of MEG resting state activity within and across brain networks as revealed by the multivariate interaction measure. NeuroImage. 2013;79:172-83. doi: http://dx.doi.org/10.1016/j.neuroimage.2013.04.062.
11. Brookes MJ, Woolrich M, Luckhoo H, Price D, Hale JR, Stephenson MC, et al. Investigating the electrophysiological basis of resting state networks using magnetoencephalography. Proceedings of the National Academy of Sciences. 2011;108(40):16783–8. doi: www.pnas.org/cgi/doi/10.1073/pnas.1112685108.
12. Siebenhühner F, Wang SH, Arnulfo G, Lampinen A, Nobili L, Palva JM, et al. Genuine cross-frequency coupling networks in human resting-state electrophysiological recordings. PLoS Biology. 2020;18(5):e3000685. doi: 10.1371/journal.pbio.3000685.
13. Zhigalov A, Arnulfo G, Nobili L, Palva S, Palva JM. Modular co-organization of functional connectivity and scale-free dynamics in the human brain. Network Neuroscience. 2017;1(2):143-65. doi: https://doi.org/10.1162/netn_a_00008.
14. Betti V, Corbetta M, de Pasquale F, Wens V, Della Penna S. Topology of functional connectivity and hub dynamics in the beta band as temporal prior for natural vision in the human brain. Journal of Neuroscience. 2018;38(15):3858-71. doi: 10.1523/JNEUROSCI.1089-17.2018.
15. Hahn A, Breakspear M, Rischka L, Wadsak W, Godbersen GM, Pichler V, et al. Reconfiguration of functional brain networks and metabolic cost converge during task performance. eLife. 2020;9:e52443. doi: 10.7554/eLife.52443.
16. Vidaurre D, Llerad A, Smithc SM, Woolrich MW. Behavioural relevance of spontaneous, transient brain network interactions in fMRI. NeuroImage. 2021;229:117713. doi: 10.1016/j.neuroimage.2020.117713.
17. Mostame P, Sadaghiani S. Oscillation-based connectivity architecture is dominated by an intrinsic spatial organization, not cognitive state or frequency. Journal of Neuroscience. 2020. doi: 10.1523/JNEUROSCI.2155-20.2020.
18. Cabral J, Kringelbach ML, Deco G. Exploring the network dynamics underlying brain activity during rest. Progress in Neurobiology. 2014;114:102-31. doi: 10.1016/j.pneurobio.2013.12.005.
19. Kringelbach ML, Cruzat J, Cabral J, Knudsen GM, Carhart-Harris R, Whybrow PC, et al. Dynamic coupling of whole-brain neuronal and neurotransmitter systems. Proceedings of the National Academy of Sciences. 2020;117(17):9566-76. doi: 10.1073/pnas.1921475117.
20. Harris KD, Thiele A. Cortical state and attention. Nature Reviews Neuroscience. 2011;12(9):509-23. doi: 10.1038/nrn3084.
21. van den Brink RL, Niuwenhuis S, Donner TH. Amplification and suppression of distinct brainwide activity patterns by catecholamines. Journal of Neuroscience. 2018;38(34):7476–91. doi: 10.1523/JNEUROSCI.0514-18.2018.
22. Cools R. Chemistry of the adaptive mind: Lessons from dopamine. Neuron. 2019;104(1):113-31. doi: 10.1016/j.neuron.2019.09.035.
23. Robbins TW, Arnsten AFT. The neuropsychopharmacology of fronto-executive function: monoaminergic modulation. Annual Review of Neuroscience. 2009;32:267-87. doi: 10.1146/annurev.neuro.051508.135535.
24. Štrac DSv, Pivac N, Mück-Šeler D. The serotonergic system and cognitive function. Translational neuroscience. 2016;7(1):35-49. doi: 10.1515/tnsci-2016-0007.

25. Lucki I. The spectrum of behaviors influenced by serotonin. Biological psychiatry. 1988;44:151–62.
26. Lee S-H, Dan Y. Neuromodulation of brain states. Neuron. 2012;76(1):109-222. doi: 10.1016/j.neuron.2012.09.012.
27. van den Brink RL, Preffer T, Donner TH. Brainstem modulation of large-scale intrinsic cortical activity correlations. Frontiers in Human Neuroscience. 2019;13:340. doi: 10.3389/fnhum.2019.00340.
28. Ferguson KA, Cardin JA. Mechanisms underlying gain modulation in the cortex. Nature Reviews Neuroscience. 2020;21:80-92. doi: 10.1038/ s41583-019-0253-y.
29. Monto S, Palva S, Voipio J, Palva JM. Very slow EEG fluctuations predict the dynamics of stimulus detection and oscillation amplitudes in humans. Journal of Neuroscience. 2008;28(33):8268 – 72. doi: 10.1523/JNEUROSCI.1910-08.2008.
30. Hiltunen T, Kantola J, Elseoud AA, Lepola P, Suominen K, Starck T, et al. Infra-slow EEG fluctuations are correlated with resting-state network dynamics in fMRI. Journal of Neuroscience. 2014;34(2):356 –62. doi: 10.1523/JNEUROSCI.0276-13.2014.
31. Linkenkaer-Hansen K, Nikouline VV, Palva JM, Ilmoniemi RJ. Long-range temporal correlations and scaling behavior in human brain oscillations. Journal of Neuroscience. 2001;21(4):1370–7.
32. Zhigalov A, Arnulfo G, Nobili L, Palva S, Palva JM. Relationship of fast-and slow-timescale neuronal dynamics in human MEG and SEEG. The Journal of Neuroscience. 2015;35(13):5385-96.
33. Poil S-S, Hardstone R, Mansvelder HD, Linkenkaer-Hansen K. Critical-state dynamics of avalanches and oscillations jointly emerge from balanced excitation/Inhibition in neuronal networks. Journal of Neuroscience. 2012;32(29):9817-23. doi: 10.1523/JNEUROSCI.5990-11.2012.
34. Thiery T, Lajnef T, Combrisson E, Dehgan A, Rainville P, Mashour GA, et al. Long-range temporal correlations in the brain distinguish conscious wakefulness from induced unconsciousness. NeuroImage. 2018;179:30–9. doi: 10.1016/j.neuroimage.2018.05.069.
35. Palva JM, Zhigalov A, Hirvonen J, Korhonen O, Linkenkaer-Hansen K, Palva S. Neuronal long-range temporal correlations and avalanche dynamics are correlated with behavioral scaling laws. Proceedings of the National Academy of Sciences, of the USA. 2013;110(9):3585–90. doi: www.pnas.org/cgi/doi/10.1073/pnas.1216855110.
36. Smit DJA, Linkenkaer-Hansen K, de Geus EJC. Long-range temporal correlations in resting-state alpha oscillations predict human timing-error dynamics. Journal of Neuroscience. 2013;33(27):11212-20. doi: 10.1523/JNEUROSCI.2816-12.2013.
37. Leppäaho E, Renvall H, Salmela E, Kere J, Salmelin R, Kaski S. Discovering heritable modes of MEG spectral power. Human Brain Mapping. 2019;40(5):1391-402. doi: 10.1002/hbm.24454.
38. Salmela E, Renvall H, Kujala J, Hakosalo O, Illman M, Vihla M, et al. Evidence for genetic regulation of the human parieto-occipital 10-Hz rhythmic activity. European Journal of Neuroscience. 2016;44:1963–71. doi: 10.1111/ejn.13300.
39. Van Pelt S, Boomsma DI, Fries P. Magnetoencephalography in twins reveals a strong genetic determination of the peak frequency of visually induced gamma-band synchronization. Journal of Neuroscience. 2012;32(10):3388-92. doi: 10.1523/JNEUROSCI.5592-11.2012.
40. Linkenkaer-Hansen K, Smit DJA, Barkil A, van Beijsterveldt TEM, Brussaard AB, Boomsma DI, et al. Genetic contributions to long-range temporal correlations in ongoing

oscillations. Journal of Neuroscience. 2007;27(50):13882–9. doi: 10.1523/JNEUROSCI.3083-07.2007.

41. Posthuma D, de Geus EJC, Boomsma DI. Perceptual speed and IQ are associated through common genetic factors. Behavior Genetics. 2001;31(6):593-602.
42. Männistö PT, Kaakkola S. Catechol-O-methyltransferase (COMT): biochemistry, molecular biology, pharmacology, and clinical efficacy of the new selective COMT inhibitors. Pharmacological reviews. 1999;51(4):593-628.
43. Parkin GM, Udawela M, Gibbons A, Scarr E, Dean B. Catechol-O-methyltransferase (COMT) genotypes are associated with varying soluble, but not membrane-bound COMT protein in the human prefrontal cortex. Journal of human genetics. 2018;63(12):1251-8. doi: 10.1038/s10038-018-0511-2.
44. Chen J, Lipska BK, Halim N, Ma QD, Matsumoto M, Melhem S, et al. Functional analysis of genetic variation in catechol-O-methyltransferase (COMT): Effects on mRNA, protein, and enzyme activity in postmortem human brain. American Journal of Human Genetics. 2004;75:807-21.
45. Fisher PM, Ozenne B, Svarer C, Adamsen D, Lehel S, Baaré WFC, et al. BDNF val66met association with serotonin transporter binding in healthy humans. Translational Psychiatry. 2017;7:e1029. doi: 10.1038/tp.2016.295.
46. Egan MF, Kojima M, Callicott JH, Goldberg TE, Kolachana BS, Bertolino A, et al. The BDNF val66met polymorphism affects activity-dependent secretion of BDNF and human memory and hippocampal function. Cell. 2003;112(2):257-69.
47. Meyer-Lindenberg A, Kohn PD, Kolachana BS, Kippenhan S, McInerney-Leo A, Nussbaum R, et al. Midbrain dopamine and prefrontal function in humans: interaction and modulation by COMT genotype. Nature neuroscience. 2005;8:594-6. doi: 10.1038/nn1438.
48. Mier D, Kirsch P, Meyer-Lindenberg A. Neural substrates of pleiotropic action of genetic variation in COMT: a meta-analysis. Molecular Psychiatry. 2010;15:918-27. doi: 10.1038/mp.2009.36.
49. Tunbridge EM, Narajos M, Harrison CH, Beresford C, Cipriani A, Harrison PJ. Which dopamine polymorphisms are functional? Systematic review and meta-analysis of COMT, DAT, DBH, DDC, DRD1–5, MAOA, MAOB, TH, VMAT1, and VMAT2. Biological Psychiatry. 2019;88:608-20. doi: 10.1016/j.biopsych.2019.05.014.
50. Zagrebelsky M, Korte M. Form follows function: BDNF and its involvement in sculpting the function and structure of synapses. Neuropharmacology. 2014;76:628e38. doi: 10.1016/j.neuropharm.2013.05.029.
51. Park H, Poo Mm. Neurotrophin regulation of neural circuit development and function. Nature Reviews Neuroscience. 2013;14(1):7-23. doi: 10.1038/nrn3379.
52. Shew WL, Yang H, Petermann T, Roy R, Plenz D. Neuronal avalanches imply maximum dynamic range in cortical networks at criticality. Journal of Neuroscience. 2009;29(49):15595–600. doi: 10.1523/JNEUROSCI.3864-09.2009.
53. Plenz D, Thiagarajan TC. The organizing principles of neuronal avalanches: cell assemblies in the cortex? Trends in Neurosciences. 2007;30(3):101-10. doi: 10.1016/j.tins.2007.01.005.
54. Deco G, Kringelbach ML, Arnatkeviciute A, Oldham S, Sabaroedin K, Rogasch NC, et al. Dynamical consequences of regional heterogeneity in the brain's transcriptional landscape. Science Advances. 2021;7(29):eabf4752. doi: 10.1126/sciadv.abf4752.
55. Priesemann V, Wibral M, Valderrama M, Pröpper R, Le Van Quyen M, Geisel T, et al. Spike avalanches in vivo suggest a driven, slightly subcritical brain state. Frontiers in systems neuroscience. 2014;8:108. doi: 10.3389/fnsys.2014.00108.

56. Hardstone R, Poil S-S, Schiavone G, Jansen R, Nikulin VV, Mansvelder HD, et al. Detrended fluctuation analysis: a scale-free view on neuronal oscillations. Frontiers in Physiology. 2012;3(Article 450):1-13. doi: 10.3389/fphys.2012.00450.
57. Palva JM, Wang SH, Palva S, Zhigalov A, Monto S, Brookes MJ, et al. Ghost interactions in MEG/EEG source space: A note of caution on inter-areal coupling measures. NeuroImage. 2018;173:632–43. doi: 10.1016/j.neuroimage.2018.02.032.
58. Yeo BTT, Krienen FM, Sepulcre J, Sabuncu MR, Lashkari D, Hollinshead M, et al. The organization of the human cerebral cortex estimated by intrinsic functional connectivity. Journal of Neurophysiology. 2011;106:1125-65. doi: 10.1152/jn.00338.2011.
59. Stephani T, Waterstraat G, Haufe S, Curio G, Villringer A, Nikulin VV. Temporal signatures of criticality in human cortical excitability as probed by early somatosensory responses. Jounal of Neuroscience. 2020;40(34):6572-83. doi: 10.1523/JNEUROSCI.0241-20.2020.
60. Palva S, Palva JM. Roles of brain criticality and multiscale oscillations in temporal predictions for sensorimotor processing. Trends in Neurosciences. 2018;41(10):729-43. doi: https://doi.org/10.1016/j.tins.2018.08.008.
61. Donhauser PW, Baillet S. Two distinct neural timescales for predictive speech processing. Neuron. 2020;105:385–93. doi: 10.1016/j.neuron.2019.10.019.
62. Bonetti L, Bruzzone SEP, Sedghi NA, Haumann NT, Paunio T, Kantojärvi K, et al. Brain predictive coding processes are associated to COMT gene Val158Met polymorphism. NeuroImage. 2021;233:117954. doi: 10.1016/j.neuroimage.2021.117954.
63. Bodenmann S, Rusterholz T, Dürr R, Stoll C, Bachmann V, Geissler E, et al. The functional Val158Met polymorphism of COMT predicts interindividual differences in brain oscillations in young men. Journal of Neuroscience. 2009;29(35):10855-62. doi: 10.1523/JNEUROSCI.1427-09.2009.
64. Garcia-Garcia M, Via M, Zarnowiec K, SanMiguel I, Escera C, Clemente IC. COMT and DRD2/ANKK-1 gene-gene interaction account for resetting of gamma neural oscillations to auditory stimulus-driven attention. PLoS ONE. 2017;12(2):e0172362. doi: 10.1371/journal.pone.0172362.
65. Chen W, Chen C, Xia M, Wu K, Chen C, He Q, et al. Interaction effects of BDNF and COMT genes on resting-state brain activity and working memory. Frontiers in human neuroscience. 2016;10:540. doi: 10.3389/fnhum.2016.00540.
66. Puig MV, Gulledge AT. Serotonin and prefrontal cortex function: Neurons, networks, and circuits. Molecular Neurobiology. 2011;44.
67. Gener T, Tauste Campo A, Alemany-González M, Nebot P, Delgado-Sallent C, Chanovas J, et al. Serotonin 5-HT1A, 5-HT2A and dopamine D2 receptors strongly influence prefronto-hippocampal neural networks in alert mice: Contribution to the actions of risperidone. Neuropharmacology. 2019;158:107743. doi: 10.1016/j.neuropharm.2019.107743.
68. Wiencke K, Horstmann A, Mathar D, Villringer A, Neumann J. Dopamine release, diffusion and uptake: A computational model for synaptic and volume transmission. PLoS Computational Biology. 2020;16(11):e1008410. doi: 10.1371/journal.pcbi.1008410.
69. Totah NKB, Logothetis NK, Eschenko O. Noradrenergic ensemble-based modulation of cognition over multiple timescales. Brain Research. 2019;1709:50-66. doi: 10.1016/j.brainres.2018.12.031.
70. Cools R, D'Esposito M. Inverted-U–shaped dopamine actions on human working memory and cognitive control. Biological Psychiatry. 2011;69:e113-e25. doi: 10.1016/j.biopsych.2011.03.028.

71. Vijayraghavan S, Wang M, Birnbaum SG, Williams GV, Arnsten AFT. Inverted-U dopamine D1 receptor actions on prefrontal neurons engaged in working memory. Nature neuroscience. 2007;10(3):376-84. doi: 10.1038/nn1846.
72. Farrell SM, Tunbridge EM, Braeutigam S, Harrison PJ. COMT Val158Met genotype determines the direction of cognitive effects produced by catechol-O-methyltransferase inhibition. Biological Psychiatry. 2012;71:538-44. doi: 10.1016/j.biopsych.2011.12.023.
73. Dosenbach NUF, Fair DA, Cohen AL, Schlaggar BL, Petersen SE. A dual-networks architecture of top-down control. Trends in Cognitive Sciences. 2008;12(3):99-105.
74. Newbold DJ, Gordon EM, Laumann TO, Seider NA, Montez DF, Gross SJ, et al. Cingulo-opercular control network and disused motor circuits joined in standby mode. Proceedings of the National Academy of Sciences. 2021;118(13):e2019128118. doi: 10.1073/pnas.2019128118.
75. Ott T, Nieder A. Dopamine and cognitive control in prefrontal cortex. Trends in Cognitive Sciences. 2019;23(3):213-34. doi: 10.1016/j.tics.2018.12.006.
76. Björklund A, Dunnett SB. Dopamine neuron systems in the brain: an update. Trends in Neurosciences. 2007;30(5):194-202. doi: 10.1016/j.tins.2007.03.006.
77. Deco G, Jirsa VK. Ongoing cortical activity at rest: Criticality, multistability, and ghost attractors. The Journal of Neuroscience. 2012;32(10):3366-75. doi: 10.1523/JNEUROSCI.2523-11.2012.
78. Daffertshofer A, Ton R, Kringelbach ML, Woolrich M, Deco G. Distinct criticality of phase and amplitude dynamics in the resting brain. NeuroImage. 2018;180:442-7. doi: 10.1016/j.neuroimage.2018.03.002.
79. Kinouchi O, Copelli M. Optimal dynamical range of exitable networks at criticality. Nature Physics. 2006;2:348-51. doi: 10.1038/nphys289.
80. Cocchi L, Gollo LL, Zalesky A, Breakspear M. Criticality in the brain: A synthesis of neurobiology, models and cognition. Progress in Neurobiology. 2017;158:132-52. doi: http://dx.doi.org/10.1016/j.pneurobio.2017.07.002.
81. Shew WL, Plenz D. The functional benefits of criticality in the cortex. The Neuroscientist. 2013;19(1):88-100. doi: 10.1177/1073858412445487.
82. Simola J, Zhigalov A, Morales-Muños I, Palva JM, Palva S. Critical dynamics of endogenous fluctuations predict cognitve flexibility in the Go/NoGo task. Scientific Reports. 2017;7:2909. doi: 10.1038/s41598-017-02750-9.
83. Schirner M, Randal McIntosh A, Jirsa V, Deco G, Ritter P. Inferring multi-scale neural mechanisms with brain network modelling. ELife. 2018;7:e28927. doi: 10.7554/eLife.28927.
84. Braun U, Harneit A, Pergola G, Menara T, Schäfer A, Betzel RF, et al. Brain network dynamics during working memory are modulated by dopamine and diminished in schizophrenia. Nature Communications. 2021;12:3478. doi: 10.1038/s41467-021-23694-9.
85. Munn BR, Müller EJ, Wainstein G, Shine JM. The ascending arousal system shapes neural dynamics to mediate awareness of cognitive states. Nature Communications. 2021;12:6016 doi: 10.1038/s41467-021-26268-x.
86. Castrén E, Monteggia LM. Brain-derived neurotrophic factor signaling in depression and antidepressant action. Biological Psychiatry. 2021;90:128–36. doi: 10.1016/j.biopsych.2021.05.008.
87. Winkel F, Ryazantseva M, Voigt MB, Didio G, Lilja A, Pou ML, et al. Pharmacological and optical activation of TrkB in Parvalbumin interneurons regulate intrinsic states to orchestrate cortical plasticity. Molecular Psychiatry. 2021. doi: 10.1038/s41380-021-01211-0.

88. Grasby KL, Jahanshad N, al. e. The genetic architecture of the human cerebral cortex. Science. 2020;367(6484):eaay6690. doi: 10.1126/science.aay6690.
89. Pusil S, López ME, Cuesta P, Bruña R, Pereda E, Maestú F. Hypersynchronization in mild cognitive impairment: the 'X' model. Brain. 2019;142:3936–50. doi: 10.1093/brain/awz320.
90. Chang CC, Chow CC, Tellier LC, Vattikuti S, Purcell SM, Lee JJ. Second-generation PLINK: rising to the challenge of larger and richer datasets. Gigascience. 2015;4(1):7. doi: 10.1186/s13742-015-0047-8.
91. Beste C, Kolev V, Yordanova J, Domschke K, Falkenstein M, Baune BT, et al. The role of the BDNF Val66Met polymorphism for the synchronization of error-specific neural networks. Journal of Neuroscience. 2010;30(32):10727-33. doi: 10.1523/JNEUROSCI.2493-10.2010.
92. Taulu S, Simola J, Kajola M. Applications of the signal space separation method. IEEE transactions on signal processing. 2005;53(9):3359-72. doi: 10.1109/TSP.2005.853302.
93. Oostenveld R, Fries P, Maris E, Schoffelen J-M. FieldTrip: Open Source Software for Advanced Analysis of MEG, EEG, and Invasive Electrophysiological Data. Computational intelligence and neuroscience. 2011;1. doi: 10.1155/2011/156869.
94. Destrieux C, Fischl B, Dale A, Halgren E. Automatic parcellation of human cortical gyri and sulci using standard anatomical nomenclature. NeuroImage. 2011;53(1):1-15. doi: 10.1016/j.neuroimage.2010.06.010.
95. Dale AM, Liu AK, Fischl BR, Buckner RL, Belliveau JW, Lewine JD, et al. Dynamic statistical parametric mapping: combining fMRI and MEG for high-resolution imaging of cortical activity. Neuron. 2000;26(1):55-67.
96. Gramfort A, Luessi M, Larson E, Engemann DA, Strohmeier D, Brodbeck C, et al. MNE software for processing MEG and EEG data. NeuroImage. 2014;86:446-60. doi: http://dx.doi.org/10.1016/j.neuroimage.2013.10.027.
97. Korhonen O, Palva S, Palva JM. Sparse weightings for collapsing inverse solutions to cortical parcellations optimize M/EEG source reconstruction accuracy. Journal of Neuroscience Methods. 2014;226:147-60. doi: http://dx.doi.org/10.1016/j.jneumeth.2014.01.031.
98. Vinck M, Oostenveld R, van Wingerden M, Battaglia F, Pennartz CMA. An improved index of phase-synchronization for electrophysiological data in the presence of volume-conduction, noise and sample-size bias. NeuroImage. 2011;55(4):1548-65. doi: 10.1016/j.neuroimage.2011.01.055.
99. Bullmore E, Sporns O. Complex brain networks: graph theoretical analysis of structural and functional systems. Nature Reviews Neuroscience. 2009;10(3):186-98. doi: 10.1038/nrn2575.
100. Schaefer A, Kong R, Gordon EM, Laumann TO, Zuo X-N, Holmes AJ, et al. Local-Global Parcellation of the Human Cerebral Cortex from Intrinsic Functional Connectivity MRI. Cerebral Cortex. 2018;28:3095–114. doi: 10.1093/cercor/bhx179.
101. Blondel VD, Guillaume J-L, Lambiotte R, Lefebvre E. Fast unfolding of communities in large networks. Journal of statistical mechanics: theory and experiment. 2008;10:P10008. doi: 10.1088/1742-5468/2008/10/P10008.

Supporting information

S1 Fig. Frequency-band clustering. Spatial similarity across frequency-bands obtained by Louvain community detection [101] for (A) oscillation amplitudes and (B) DFA exponents averaged across participants (N = 82). The clustering on spatial similarity yielded the frequency–frequency-band clusters of theta (θ, 3–7 Hz), alpha (α, 8–14 Hz), beta (β, 14–30 Hz), and gamma (γ, 30–60 Hz) bands. The color scales indicate the correlation coefficients.

S2 Fig. Whole brain averaged oscillation amplitudes, DFA and phase synchronization. Box plots of A, DFA and wPLI averaged over theta (θ, 3–7 Hz), alpha (α, 8–14 Hz), beta (β, 14–30 Hz), and gamma (γ, 30–60 Hz) frequency bands separately for each *COMT* (Val/Val in purple n = 18, Val/Met in turquoise n = 48, and Met/Met in orange n = 16) and *BDNF* polymorphism (Val/Val in purple n = 66 and combined Val/Met & Met/Met in orange n = 16) groups. The box ends indicate the lower quartile (Q1, 25th percentile) and upper quartile (Q3, 75th percentile). The central notches denote the median, and the whiskers correspond to the range of Q1 – 1.5 * IQR and Q3 + 1.5 * IQR (where IQR is the inter-quartile range) and give roughly a 95% CI for comparing the medians. Asterisks denote significant group differences (*: $p < 0.05$, *: $p < 0.01$, t-test with unequal variances).

S3 Fig. Mean oscillation amplitudes for *COMT* polymorphism groups. Mean amplitudes separately for each *COMT* (Val/Val, Val/Met, and Met/Met) polymorphism group averaged over theta (θ, 3–7 Hz), alpha (α, 8–14 Hz), beta (β, 14–30 Hz), and gamma (γ, 30–60 Hz) frequency bands plotted on inflated cortical surface. The color indicates the strength of the oscillations. Note that the scales vary across the frequency bands.

1061

1062 **S4 Fig. Mean oscillation amplitudes for *BDNF* polymorphisms.** Mean amplitudes separately for
1063 each *BDNF* polymorphism (Val/Val and Met-carriers) group averaged over theta (θ, 3–7 Hz), alpha
1064 (α, 8–14 Hz), beta (β, 14–30 Hz), and gamma (γ, 30–60 Hz) frequency bands plotted on inflated
1065 cortical surface. The color indicates the strength of the oscillations. Note that the scales vary across
1066 the frequency bands.

1067

1068 **S5 Fig. The functional subsystems.** Cortical parcels of the Destrieux atlas [94] plotted on inflated
1069 cortical surface. Color indicates the functional subsystems defined by fMRI functional connectivity
1070 [58].

1071

1072 **S6 Fig. Mean oscillation amplitudes across the functional subsystems.** Box plots of A averaged
1073 over the functional subsystems across the frequency bands: theta (θ, 3–7 Hz), alpha (α, 8–14 Hz),
1074 beta (β, 14–30 Hz), and gamma (γ, 30–60 Hz) and separately for each *COMT* (Val/Val, Val/Met,
1075 and Met/Met, upper panels) and each *BDNF* (Val/Val and Met-carriers, lower panels)
1076 polymorphism group. Abbreviations of the functional subsystems as in S5 Fig and box plot details
1077 as in S2 Fig.

1078

1079 **S7 Fig. Mean LRTCs for *COMT* polymorphisms.** Mean DFA exponents are plotted separately
1080 for each *COMT* (Val/Val, Val/Met, and Met/Met) group, averaged over theta (θ, 3–7 Hz), alpha (α,
1081 8–14 Hz), beta (β, 14–30 Hz), and gamma (γ, 30–60 Hz) frequency bands plotted on inflated cortical
1082 surface. The color indicates the strength of the DFA exponents. Note that the scales vary across the
1083 frequency bands.

1084

1085 **S8 Fig. Mean LRTCs for *BDNF* polymorphisms.** Mean DFA exponents are plotted separately
1086 for each *BDNF* polymorphism (Val/Val and Met-carriers) groups averaged over theta (θ, 3–7 Hz),
1087 alpha (α, 8–14 Hz), beta (β, 14–30 Hz), and gamma (γ, 30–60 Hz) frequency bands plotted on
1088 inflated cortical surface. The color indicates the strength of the DFA exponents. Note that the scales
1089 vary across frequency bands.
1090
1091 **S9 Fig. Mean DFA exponents across the functional subsystems.** Box plots of DFA exponents
1092 averaged over the functional subsystems defined by fMRI functional connectivity across the
1093 frequency bands: theta (θ, 3–7 Hz), alpha (α, 8–14 Hz), beta (β, 14–30 Hz), and gamma (γ, 30–60
1094 Hz) and separately for each *COMT* (Val/Val, Val/Met, and Met/Met, upper panels) and each *BDNF*
1095 (Val/Val and Met-carriers, lower panels) polymorphism groups. Abbreviations of the functional
1096 subsystems as in S5 Fig and box plot details as in S2 Fig.
1097
1098 **S10 Fig. Co-localization of oscillation amplitudes and LRTCs.** Cortical parcels in which
1099 amplitudes and DFA exponents were significantly larger for *COMT* Val/Met than Met/Met
1100 polymorphism groups in θ (3–7 Hz, upper left panel) and in β-γ (20–60 Hz, lower left panel) band,
1101 and for *BDNF* Val homozygotes than Met-carriers in θ (upper right panel), as well as for *COMT*
1102 Val/Met than Val/Val polymorphism groups in β-γ (lower right panel). The color indicates the
1103 difference in oscillation amplitudes (red) and DFA exponents (blue), as well as their joint effects
1104 (purple).
1105
1106 **S11 Fig. Phase synchronization associated with *COMT* and *BDNF* polymorphisms.** The mean
1107 phase-synchronization within and among functional Yeo subsystems across the whole brain in the
1108 canonical frequency bands for the *COMT* Val/Val, Val/Met and Met/Met polymorphism groups

and the *BDNF* Val/Val alleles and Met carriers. Inter-areal phase phase-synchrony was estimated between and within functional subsystems using the weighted phase-lag index (wPLI), of which the strength is indicated by the color scales. No differences in inter-areal phase coupling were found between *COMT* polymorphisms. *BDNF* Val/Val alleles showed stronger synchronization than Met carriers particularly in the α, β and γ bands, these differences are shown in Fig 4C. Note that the scales vary across the frequency bands. Abbreviations of the functional subsystems as in S5 Fig.

S12 Fig. Hemispheric phase synchronization for the *BDNF* polymorphism groups. The differences in the mean phase synchronization, as estimated with wPLI, within and between functional subsystems separately for left-, right- and cross-hemispheric connections. *BDNF* Val/Val homozygotes had stronger phase synchronization compared to Met-carriers averaged over frequency bands. Color indicates the Val > Met difference in mean phase-synchronization. Stars denote network pairs where the group difference was significant (Kruskal-Wallis, *: $p < 0.05$, uncorrected, **: $p < 0.01$, corrected with Benjamini-Hochberg). Abbreviations of the functional subsystems as in S5 Fig.

S13 Fig. Correlations of local and global synchronization with LRTCs. Box plots of correlations of between A and wPLI with DFA exponents averaged over theta (θ, 3–7 Hz), alpha (α, 7–14 Hz), beta (β, 14–30 Hz), and gamma (γ, 30–60 Hz) frequency bands. Correlations are shown separately for each *COMT* (Val/Val, Val/Met, and Met/Met, upper panels) and each *BDNF* (Val/Val and Met-carriers, lower panels) polymorphism group. Box plot details as in S2 Fig.

S1 Table. Mean sample characteristics (SD in parentheses) by the *COMT* polymorphisms.

S2 Table. Mean sample characteristics (SD in parenthesis) by the *BDNF* polymorphisms.

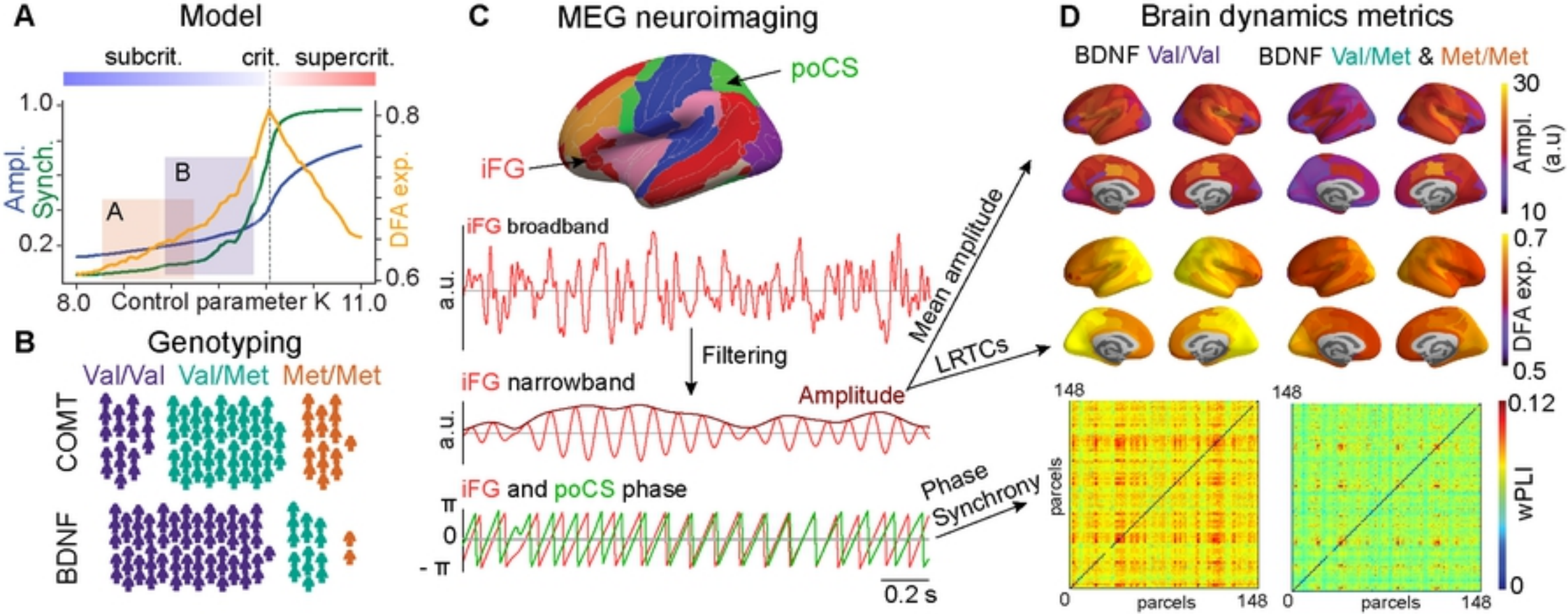
A
Model
subcrit.
crit.
supercrit.
1.0
0.2
Ampl.
Synch.
0.8
0.6
DFA exp.
A
B
8.0
Control parameter K
11.0
B
Genotyping
Val/Val
Val/Met
Met/Met
COMT
BDNF
C
MEG neuroimaging
poCS
iFG
iFG broadband
a.u.
Filtering
iFG narrowband
a.u.
Amplitude
iFG and poCS phase
π
0
- π
0.2 s
Mean amplitude
LRTCs
Phase Synchrony
D
Brain dynamics metrics
BDNF Val/Val
BDNF Val/Met & Met/Met
30
10
Ampl. (a.u)
0.7
0.5
DFA exp.
148
parcels
0
parcels
148
0.12
0
wPLI

Fig 1

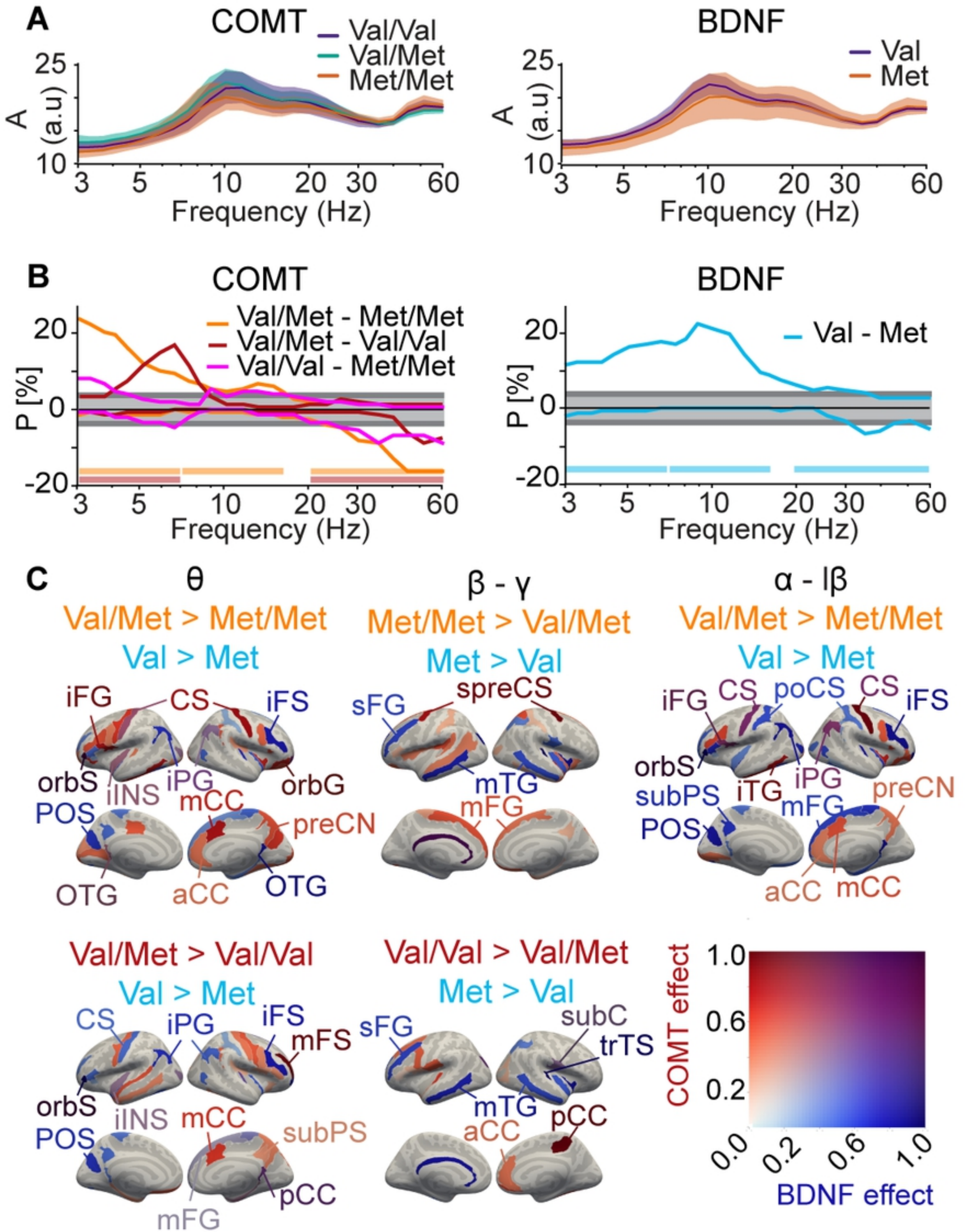
A
COMT
Val/Val
Val/Met
Met/Met
A (a.u)
Frequency (Hz)
BDNF
Val
Met
B
COMT
Val/Met - Met/Met
Val/Met - Val/Val
Val/Val - Met/Met
P [%]
BDNF
Val - Met
C
θ
Val/Met > Met/Met
Val > Met
iFG
CS
iFS
orbS
iINS
iPG
orbG
POS
mCC
preCN
OTG
aCC
β - γ
Met/Met > Val/Met
Met > Val
sFG
spreCS
mTG
mFG
α - lβ
Val/Met > Met/Met
Val > Met
iFG
CS
poCS
CS
iFS
orbS
subPS
iTG
iPG
preCN
POS
mFG
aCC
mCC
Val/Met > Val/Val
Val > Met
CS
iPG
iFS
mFS
orbS
iINS
mCC
POS
subPS
pCC
mFG
Val/Val > Val/Met
Met > Val
sFG
subC
trTS
mTG
pCC
aCC
COMT effect
BDNF effect
1.0
0.6
0.2
0.0

Fig 2

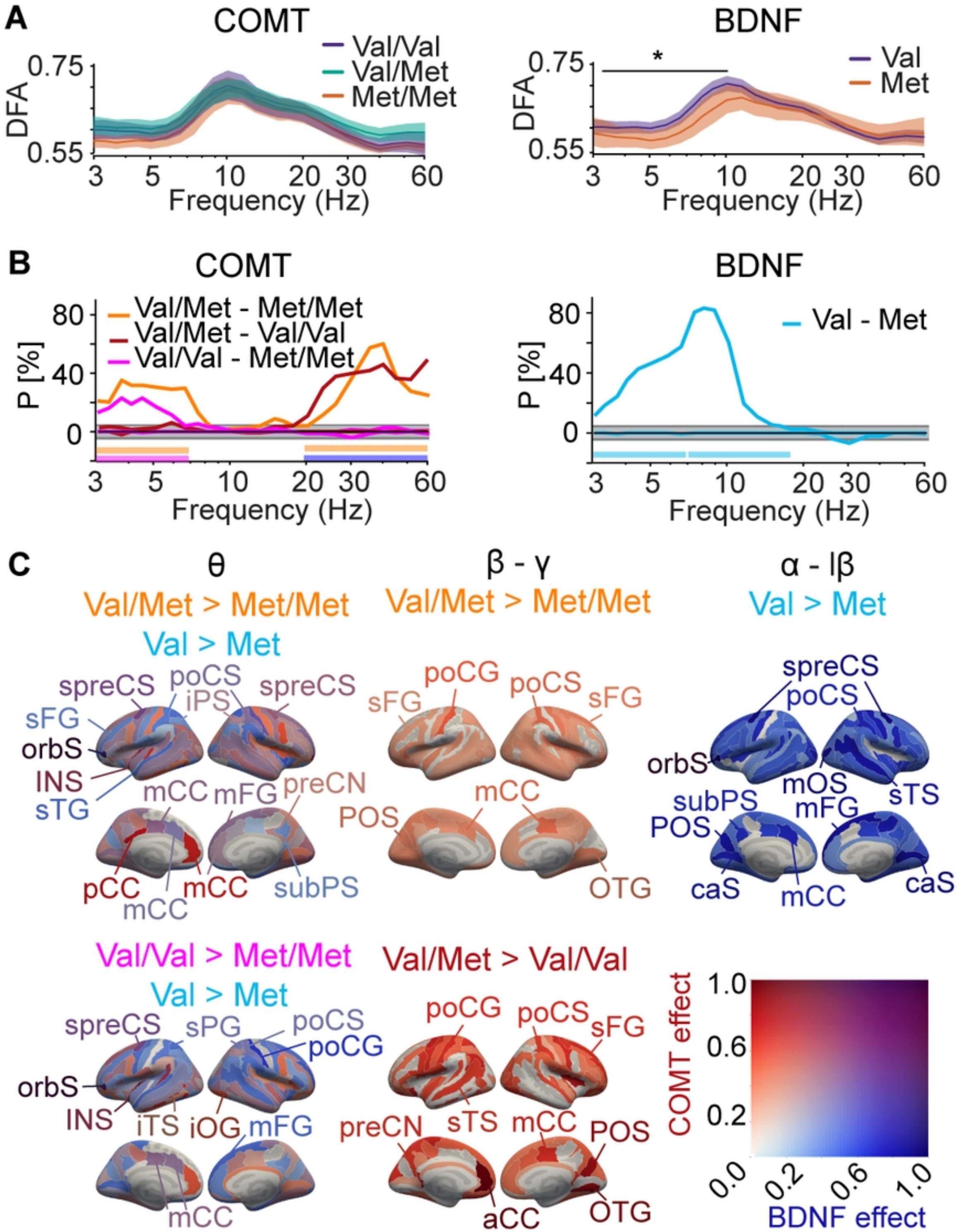
A
COMT
Val/Val
Val/Met
Met/Met
DFA
0.75
0.55
3 5 10 20 30 60
Frequency (Hz)
BDNF
*
Val
Met
B
COMT
Val/Met - Met/Met
Val/Met - Val/Val
Val/Val - Met/Met
P [%]
80
40
0
Frequency (Hz)
BDNF
Val - Met
C
θ
Val/Met > Met/Met
Val > Met
spreCS
poCS
iPS
sFG
orbS
INS
sTG
mCC
mFG
preCN
pCC
subPS
β - γ
Val/Met > Met/Met
poCG
POS
OTG
α - lβ
Val > Met
spreCS
poCS
orbS
mOS
sTS
subPS
mFG
POS
caS
Val/Val > Met/Met
Val > Met
sPG
poCG
iTS
iOG
Val/Met > Val/Val
aCC
COMT effect
BDNF effect
1.0
0.6
0.2
0.0

Fig 3

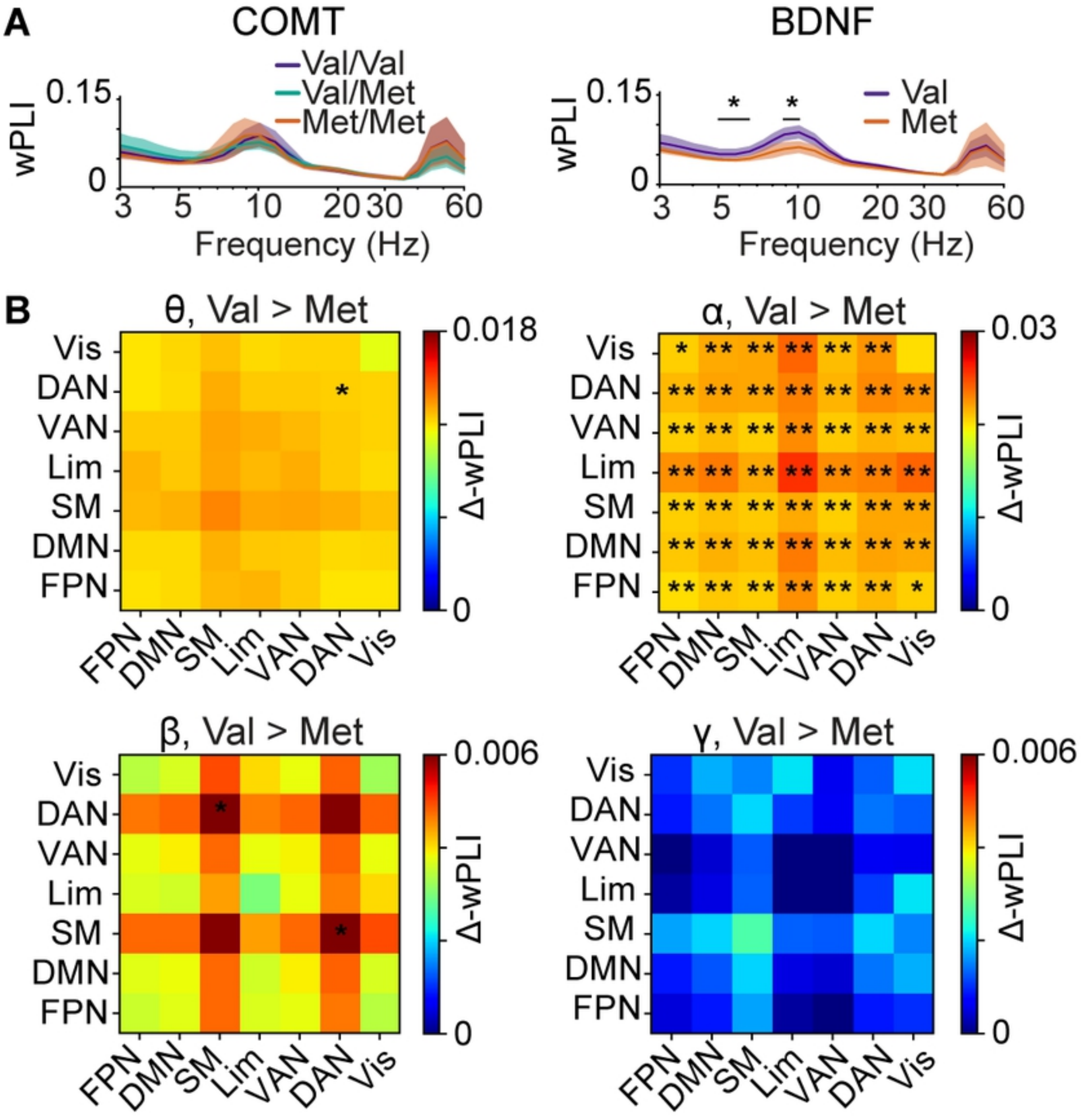
A
COMT
Val/Val
Val/Met
Met/Met
wPLI
0.15
0
3
5
10
20
30
60
Frequency (Hz)
BDNF
Val
Met
*
*
B
θ, Val > Met
α, Val > Met
β, Val > Met
γ, Val > Met
Vis
DAN
VAN
Lim
SM
DMN
FPN
0.018
0.03
0.006
Δ-wPLI

Fig 4

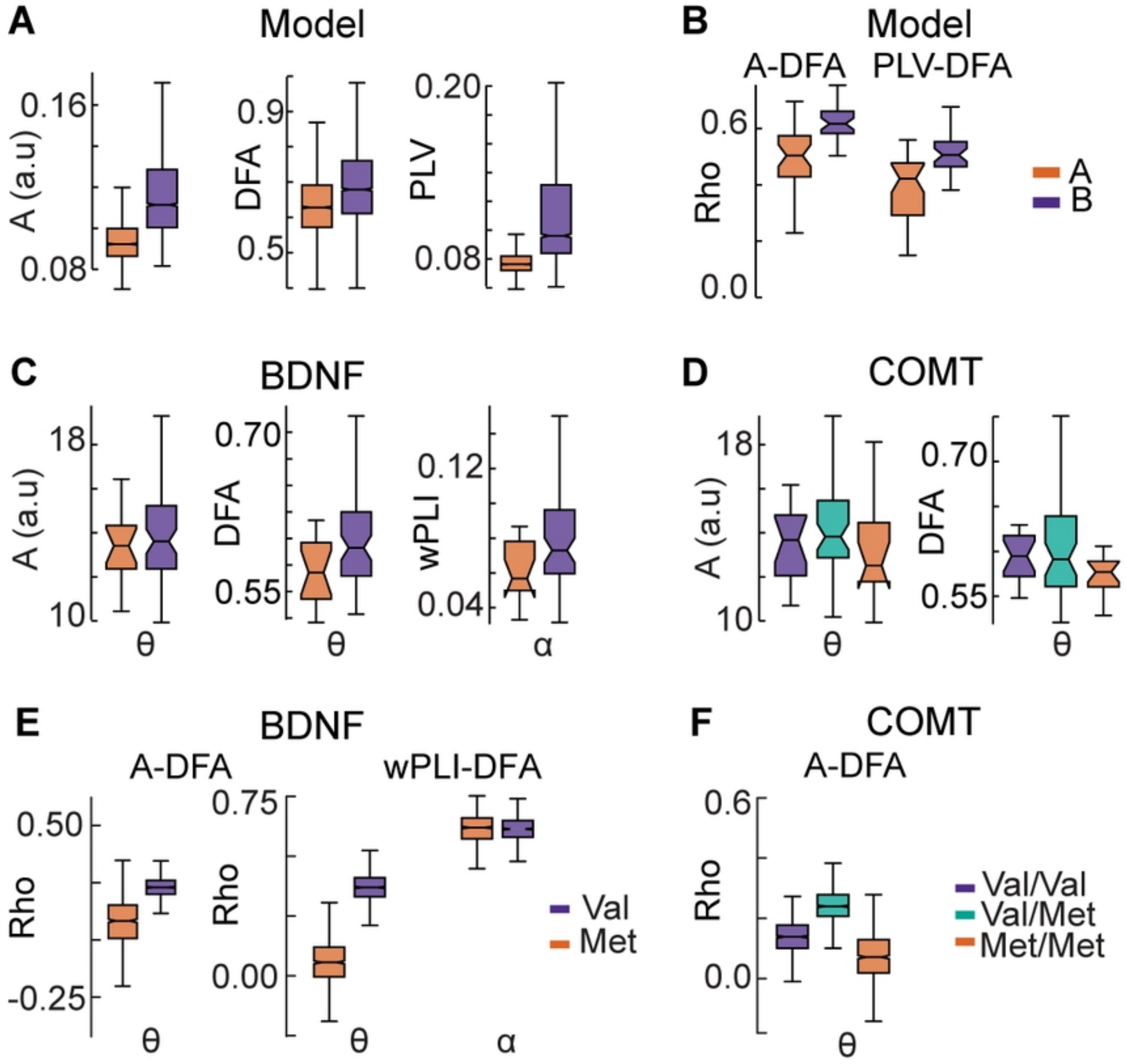
A
Model
A (a.u)
0.16
0.08
DFA
0.9
0.5
PLV
0.20
0.08
B
Model
A-DFA
PLV-DFA
Rho
0.6
0.0
A
B
C
BDNF
A (a.u)
18
10
θ
DFA
0.70
0.55
θ
wPLI
0.12
0.04
α
D
COMT
A (a.u)
18
10
θ
DFA
0.70
0.55
θ
E
BDNF
A-DFA
Rho
0.50
-0.25
θ
wPLI-DFA
Rho
0.75
0.00
θ
α
Val
Met
F
COMT
A-DFA
Rho
0.6
0.0
θ
Val/Val
Val/Met
Met/Met

Fig 5